Journal of Orthopaedic Surgery and Research

RESEARCH ARTICLE

Open Access

mir-744-5p inhibits cell growth and angiogenesis in osteosarcoma by targeting NFIX

Lin Xie[1†], Wei Li[1†] and Yu Li[2*]

Abstract

Background Osteosarcoma (OS) is a malignant bone tumor that commonly occurs in children and adolescents under the age of 20. Dysregulation of microRNAs (miRNAs) is an important factor in the occurrence and progression of OS. MicroRNA miR-744-5p is aberrantly expressed in various tumors. However, its roles and molecular targets in OS remain unclear.

Methods Differentially expressed miRNAs in OS were analyzed using the Gene Expression Omnibus dataset GSE65071, and the potential hub miRNA was identified through weighted gene co-expression network analysis. Quantitative real-time PCR (qRT-PCR) was used to detect the expression of miR-744-5p in OS cell lines. In vitro experiments, including CCK-8 assays, colony formation assays, flow cytometry apoptosis assays, and tube formation assays, were performed to explore the effects of miR-744-5p on OS cell biological behaviors. The downstream target genes of miR-744-5p were predicted through bioinformatics, and the binding sites were validated by a dual-luciferase reporter assay.

Results The lowly expressed miRNA, miR-744-5p, was identified as a hub miRNA involved in OS progression through bioinformatic analysis. Nuclear factor I X (NFIX) was confirmed as a direct target for miR-744-5p in OS. In vitro studies revealed that overexpression of miR-744-5p could restrain the growth of OS cells, whereas miR-744-5p inhibition showed the opposite effect. It was also observed that treatment with the conditioned medium from miR-744-5p-overexpressed OS cells led to poorer proliferation and angiogenesis in human umbilical vein endothelial cells (HUVECs). Furthermore, NFIX overexpression restored the suppression effects of miR-744-5p overexpression on OS cell growth and HUVECs angiogenesis.

Conclusion Our results indicated that miR-744-5p is a potential tumor-suppressive miRNA in OS progression by targeting NFIX to restrain the growth of OS cells and angiogenesis in HUVECs.

Keywords Osteosarcoma, miR-744-5p, NFIX, Angiogenesis, WGCNA

†Lin Xie and Wei Li contributed equally to this work.

*Correspondence:
Yu Li
gurouliu2021@126.com
[1]Department of Rehabilitation Medicine, Yantai Yuhuangding Hospital, Yantai, Shandong 264000, China
[2]First Ward of Trauma Orthopaedics, Yantai Shan Hospital, Yantai, Shandong 264003, China

© The Author(s) 2024. **Open Access** This article is licensed under a Creative Commons Attribution-NonCommercial-NoDerivatives 4.0 International License, which permits any non-commercial use, sharing, distribution and reproduction in any medium or format, as long as you give appropriate credit to the original author(s) and the source, provide a link to the Creative Commons licence, and indicate if you modified the licensed material. You do not have permission under this licence to share adapted material derived from this article or parts of it. The images or other third party material in this article are included in the article's Creative Commons licence, unless indicated otherwise in a credit line to the material. If material is not included in the article's Creative Commons licence and your intended use is not permitted by statutory regulation or exceeds the permitted use, you will need to obtain permission directly from the copyright holder. To view a copy of this licence, visit http://creativecommons.org/licenses/by-nc-nd/4.0/.

Introduction

Osteosarcoma (OS) is a malignant tumor of bone that develops from primitive transformed cells of mesenchymal origin and usually occurs in the long diaphyseal region [1]. OS can occur in people of any age; however, children and adolescents have a high incidence of it [2]. Although advances achieved in OS treatment including neoadjuvant chemotherapy, radiotherapy, and surgical resection have improved survival rates in OS patients, about 30% of patients without metastatic diseases subsequently develop metastasis, which often results in poor prognosis [3, 4]. Therefore, it is urgent to explore the underlying molecular mechanism involved in OS progression, which might provide potential targets for the diagnosis and treatment of OS.

Currently, microRNAs (miRNAs) have drawn increasing attention in the research on OS progression [5, 6]. MiRNAs are short, single-stranded non-coding RNA molecules at a length of about 22 nucleotides [7]. They cannot encode proteins but can negatively regulate their target genes' expression by binding to their 3'-untranslated regions. Due to this property, miRNAs are involved in a variety of biological processes [8–10]. Numerous studies have revealed that miRNAs play crucial roles in OS progression. MiR-188-5p has been revealed as a suppressive miRNA in OS by target-degrading cyclin T2 [11]. MiR-133b exerts suppressor activities in OS by directly targeting the fibroblast growth factor receptor 1 [12]. Therefore, miRNAs play essential roles in OS development and more investigations on their functional roles and molecular mechanisms are required.

Nowadays, many studies identify prognostic or therapeutic markers by analyzing high-throughput sequencing data. Besides, a variety of bioinformatic approaches are applied to understand the mechanisms underlying these data [13–15]. Weighted gene coexpression network analysis (WGCNA) is a commonly used bioinformatics tool for studying the structure and function of large-scale biomolecular networks. It can also be used to identify hub genes in networks and provide interpretation for molecular interactions [16]. For instance, Tian et al. identified OS metastasis-associated genes by WGCNA [17]. Therefore, the use of WGCNA can make contributions to exploring miRNAs that are critical for OS progression.

We screened miR-744-5p as a key miRNA in OS via WGCNA in the current study. The abnormal expression of miR-744-5p was recognized to be related to the formation and metastasis of ovarian cancer [18], lung squamous cell carcinoma [19], multiple myeloma [20] and many other cancers [21–23]. In OS, miR-744-5p showed tumor suppressive effects by negatively regulating transforming growth factor-beta 1 [24]. However, little is known about the role and molecular mechanism of miR-744-5p in OS progression.

Nuclear factor I X (NFIX), a nuclear factor I family member, has been reported to play important roles in carcinogenesis and tumor progression [25, 26]. NFIX could transcriptionally induce the Ezrin expression to the enhanced migration of glioblastoma cells [27]. Another study reported that NFIX could promote metastasis in lung cancer [28]. However, the role of NFIX in OS has not yet been reported. A previous study revealed that miR-744-5p promotes programmed cell death in ovarian cancer by targeting NFIX [18]. This suggested a molecular mechanism that miR-744-5p targets NFIX to suppress tumor growth in OS, although this has not been verified.

In this work, we identified miR-744-5p, which is downregulated in OS, through WGCNA. In vitro studies were designed to identify the function roles of miR-744-5p in OS cell growth and human umbilical vein endothelial cells (HUVECs) angiogenesis. Additionally, the regulation of miR-744-5p on NFIX in OS cells was also explored. Our study identified the miR-744-5p/NFIX axis as a novel regulator in OS progression. Therefore, targeting the miR-744-5p/NFIX axis may be a potential therapeutic approach for suppressing OS progression.

Methods

Microarray data

The miRNA microarray data came from the Gene Expression Omnibus dataset GSE65071 [29], which contains plasma samples from 20 OS patients and 15 healthy individuals. The expression profiling of miRNAs was obtained from the Exiqon miRNome platform GPL19631. The k-nearest neighbor algorithm was used to fill in the missing data. Then the data was normalized for subsequent WGCNA.

WGCNA

The OS-associated miRNAs were identified through the construction of miRNA co-expression networks using WGCNA [16]. First, a similarity matrix was constructed by calculating the absolute value of the Pearson correlation coefficient. The independence and the relevant degree of miRNA pairs in co-expression modules were calculated by the gradient method, with power values ranging from 1 to 20. A soft-thresholding power β was selected where the correlation index reached 0.9 (R^2 value ≥ 0.90). Next, all adjacencies were transformed into a topological overlap matrix. Then, the community dissimilarity index of these miRNAs was analyzed and a hierarchical clustering tree was identified. Based on dynamic cut tree criteria, we set a cut height of 0.95 and a minimal module size of 3. After the classification of gene modules, the module eigenvectors of each module were calculated along with clinical traits and shown as a heatmap. The modules closely associated with the disease condition are considered to be the key modules. Gene

significance (GS) represents the correlation of individual genes with disease traits. Module membership (MM) shows the relationship between module eigengenes and expression values of genes. The correlation factor of MM with GS was evaluated by Pearson correlation analysis to verify the intra-modular connectivity.

Enrichment analysis

The Gene Ontology (GO) functional and Kyoto Encyclopedia of Genes and Genomes (KEGG) pathway enrichment analysis were performed on miR-744-5p-targeted genes clusterProlifer [30]. The threshold was set at a *P* value and Q value < 0.05.

Cell culture

The 143B and U2OS human osteosarcoma cell lines, as well as the hFOB1.19 osteoblast cell line, were purchased from Shanghai FuHeng Biology (Shanghai, China). The HUVECs were purchased from the American Type Culture Collection (Manassas, USA). The 143B and U2OS cells were cultured in Dulbecco's Modified Eagle Medium, the hFOB1.19 cells were cultured in Dulbecco's Modified Eagle Medium/Nutrient Mixture F-12 with 1% penicillin/streptomycin and 10% fetal bovine serum, and the HUVECs were cultured in Endothelial Cell Growth Medium. All cells were maintained at 37℃ with 5% CO_2.

Cell transfection

The miR-744-5p mimics, miR-744-5p inhibitor, NFIX overexpression plasmid, and their negative controls were obtained from GenePharma (Shanghai, China). Briefly, the miR-744-5p mimics were synthesized according to the mature miR-744-5p sequence (miRbase ID: MIMAT0004945), and the miR-744-5p inhibitor was the reverse complementary sequence of the mature miR-744-5p. As to the NFIX overexpression vector, the full-length NFIX coding sequence was amplified using polymerase chain reaction (PCR) with the following sequences: Forward: 5' CGGGGTACCGCCACCATGT ACTCCCCGTACT-3' and Reverse: 5'-CCGCTCGAG TCAGAGGAACCAGGACTG-3'. Then, the amplification products were inserted into pcDNA3.1 vectors to construct the NFIX overexpression vector with the help of the KpnI and XhoI endonucleases.

For cell transfection, the cells were pre-incubated at 37℃ for 12 h and then transfected at 50–70% confluence. Cells were transfected with miR-744-5p mimics (50 nM), mimics-NC (50 nM), miR-744-5p inhibitor (100 nM), inhibitor-NC (100 nM), empty vector (1 μg), and NFIX overexpression vector (1 μg) using the Lipofectamine 3000 (Thermo Fisher Scientific, USA) under the manufacturer's protocol. 48 h after the transfection, the cells were harvested for the following experiments.

Table 1 Primer sequences of qRT-PCR

ID		Primers for qRT-PCR (5'-3')
miR-744-5p	Forward	TGCGGGGCTAGGGCTA
	Reverse	GGCCCAGTGTTCAGACTAC
NFIX	Forward	CGGCTCTACAAGTCGCCTC
	Reverse	GCAGTGGTTTGATGTCCGC
GAPDH	Forward	ACCTGACCTGCCGTCTAGAA
	Reverse	TCCACCACCTGTTGCTGTA
U6	Forward	CTCGCTTCGGCAGCACA
	Reverse	AACGCTTCACGAATTTGCGT

Quantitative real-time PCR (qRT-PCR)

Total RNA was isolated and purified using QIAzol lysis solution (Qiagen, Germany) and miRNeasy kit (Qiagen). Then, cDNA was synthesized using the QuantiTect RT Kit (Qiagen) and miScript II RT Kit (Qiagen). RNA was detected by using the LightCycler 480 SYBR Green I Master kit (Roche, Switzerland) with primer sequences listed in Table 1. RNA was amplified through thermocycling with 10 min of initial denaturation at 95 °C, 40 cycles of amplification for 20 s per cycle, and 1 min of annealing at 60 °C. Data quantification was normalized by the $2^{-\Delta\Delta CT}$ method with GAPDH or U6 as internal references.

Cell viability

The Cell Counting Kit-8 (CCK-8) assay was applied to test cell viability. 143B and U2OS cells were split and transferred into 96-well plates with about 3×10^3 cells per well. For HUVECs, as previously reported [31], were mixed with OS cells conditioned medium (CM) and transferred into 96-well plates (2×10^3 cells/well) at 37℃, 5% CO_2.

Cells were harvested at 0, 24, 48, 72, and 96 h after incubation. Subsequently, 10 μL of CCK-8 solution (Dojindo, Japan) was added to each well and cultured at 37℃ for 2 h. Cell viability was determined by measuring the optical density values at 450 nm using a microplate reader.

Colony formation assay

The treated 143B and U2OS cells were digested and transferred into 6-well plates with 1×10^3 cells per well. After incubation for 2 weeks, cells were fixed using methyl alcohol and stained to visualize colonies.

Cell apoptosis

The Annexin V Apoptosis Detection Kit (BD Biosciences, USA) was applied for cell apoptosis detection. Cell pellets were resuspended in 500 μL binding buffer and incubated with 5 μL FITC Annexin V and 5 μL Propidium Iodide for 1 h. Subsequently, the apoptotic cells were detected using flow cytometry.

Tube formation assay

HUVECs were cultured with the OS cells' CM for 24 h before conducting the tube formation assay. A 96-well tray was coated by 50 μL Matrigel Basement Membrane Matrix (Corning, USA) per well at 37 ℃ for 30 min. The pre-treated HUVECs (2×10^4/well) were added into the pre-coated 96-well tray and incubated at 37℃ for 4 h. Finally, tube formation results were observed under a microscopy.

Dual-luciferase reporter assay

Partial sequences (300 bp) of NFIX 3' untranslated regions (3'UTR) containing wild type (WT) or mutant (MUT) miR-744-5p binding sites were subcloned into psiCHECK-2 vector by GenePharma, to establish the NFIX WT vectors (C09005) and NFIX MUT vectors (C09006), respectively. Then, 143B cells in 24-well plates were co-transfected with 0.1 μg of corresponding reporter vector and 50 nM miR-744-5p mimics or mimic NC using Lipofectamine 3000 (Thermo Fisher Scientific). 48 h after transfection, cells were lysed and luciferase activities were measured using a Dual-Luciferase Reporter Assay System (Promega, USA).

Western blot

Briefly, total proteins from the cells were lysed in radioimmunoprecipitation assay buffer (Boster Bio, China) and quantified using a bicinchoninic acid assay kit (KeyGEN BioTECH, China). Next, 40 μg of protein was isolated by 10% sodium dodecyl sulfate-polyacrylamide gel electrophoresis and transferred onto polyvinylidene fluoride membranes (Millipore, USA). After being blocked with 5% non-fat milk, the membranes were incubated with primary antibodies at 4℃ overnight and corresponding secondary antibodies at 37℃ for 2 h. Finally, the protein bands were detected by chemiluminescence. The primary antibodies used were as follows: anti-NFIX (Nbp2-15038, 1:1000, Novus Biologicals); anti-GAPDH (AB9485, 1:2000, Abcam).

Statistical analysis

All data were expressed as mean±standard deviation from at least three reduplicate experiments. Group comparisons were achieved by using Student's *t*-test or one-way analysis of variance followed by the Tukey test. A significance level of $P<0.05$ was considered statistically significant.

Results

Identification of WGCNA modules associated with OS

As WGCNA is recommended to try on a dataset of more than 15 samples (https://labs.genetics.ucla.edu/horvath/CoexpressionNetwork/Rpackages/WGCNA/faq.html), we used the dataset GSE65071 (35 samples) to establish the miRNA co-expression networks. Cluster analysis was carried out and the clustering tree was shown in Fig. 1A, where the hierarchical clustering dendrograms showed no outliers. The value of paired miRNA correlation was explored for network construction, followed by the construction of the adjacency matrix and topological overlap matrix. According to the result (Fig. 1B), the soft-thresholding power was set as 10, and 7 modules were obtained (Fig. 1C). From the analysis diagram of module eigengenes (Fig. 1D), we observed that the green module ($r=0.54$, $P=9\times10^{-4}$), yellow module (r = -0.45, $P=0.007$), turquoise module (r = -0.99, $P=3\times10^{-30}$), blue module (r = -0.6, $P=1\times10^{-4}$), and red module (r = -0.63, $P=6\times10^{-5}$) were closely associated with OS. The turquoise module showed the closest connection to OS and therefore presented clinical significance. MM and GS were also found to be positively correlated with disease status (Fig. 1E).

Identification of hub miRNA in turquoise module

A co-expression network of the turquoise module was constructed. It was found that miR-744-5p was the highly connected hub miRNA in the turquoise module (Fig. 2A). Further KEGG enrichment analysis results indicated that miR-744-5p was associated with some cancer-related pathways, such as the AMPK signaling pathway and the mTOR signaling pathway (Fig. 3A; Table 2). GO enrichment analysis also confirmed the involvement of miR-744-5p in cell junction, branching morphogenesis of epithelial cast, etc. (Fig. 3B; Tables 3, 4 and 5). These bioinformatics analysis results indicated that the hub miRNA miR-744-5p might play a regulatory role in OS progression.

Mir-744-5p inhibited the cell viability of osteosarcoma cells and the tube formation of HUVECs

MiR-744-5p expression in OS cells was examined using qRT-PCR assay, which showed significantly reduced expression in OS cells compared with osteoblasts (Fig. 4A). Next, to investigate the involvement of miR-744-5p in OS carcinogenesis, we transfected 143B cells and U2OS cells with miR-744-5p mimics and inhibitors (Fig. 4B). After transfection, cell viability was determined by CCK-8 and colony formation assays. We observed that miR-744-5p overexpression observably reduced the cell viability of 143B and U2OS cells, while miR-744-5p inhibition observably promoted the cell viability (Fig. 4C-D). Additionally, cell apoptosis after transfection was detected. Overexpression of miR-744-5p promoted the apoptosis rates in OS cells, while the knockdown of miR-744-5p inhibited apoptosis in OS cells (Fig. 4E).

Considering that GO enrichment analysis showed the involvement of miR-744-5p in angiogenesis (Table 3), we investigated the effects of miR-744-5p on tube formation

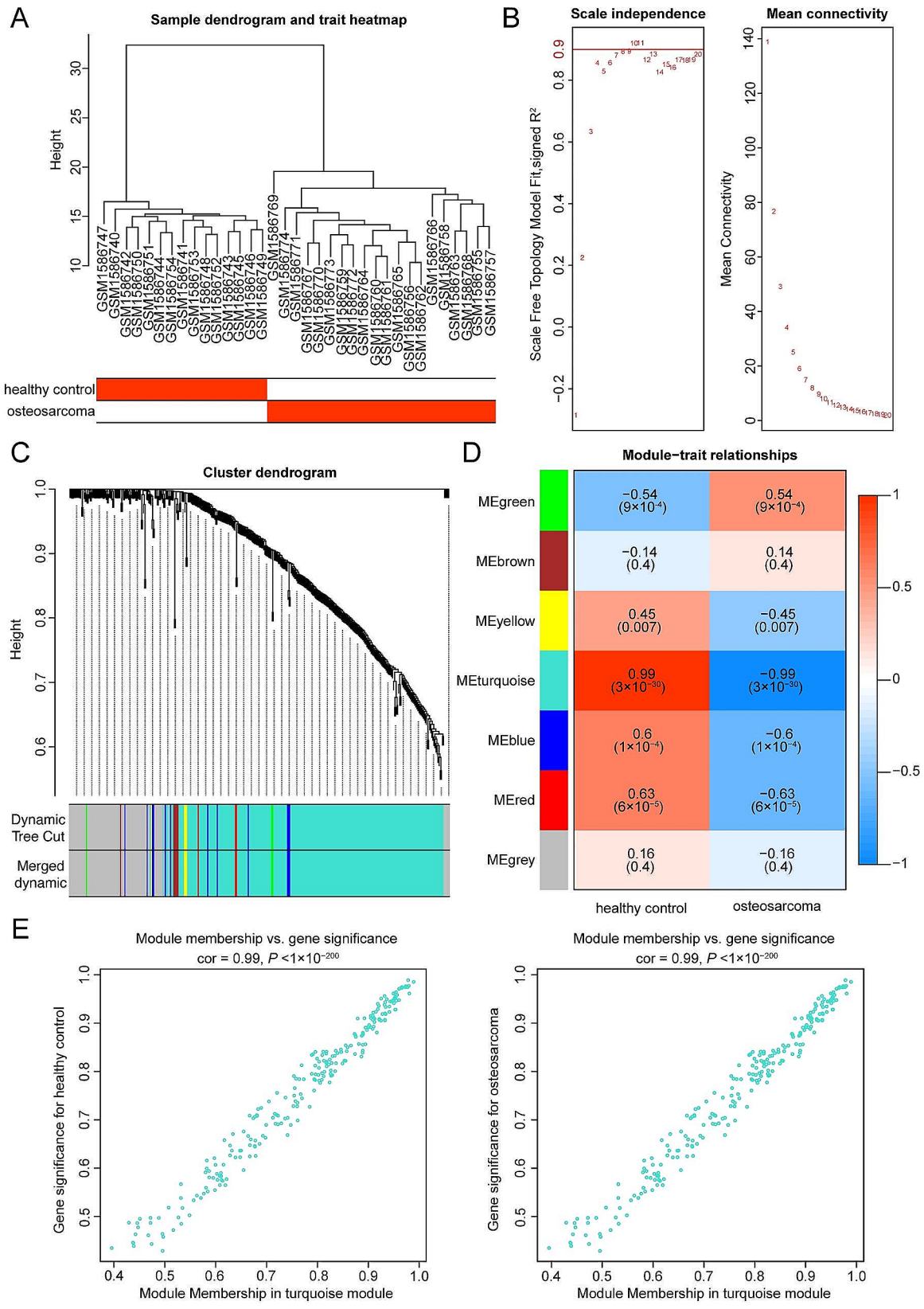

Fig. 1 Dataset network construction and significant modules identification. (**A**) Hierarchical clustering plot of GSE65071. (**B**) Calculation of adjacency matrix weighting power. (**C**) Clustering dendrograms of co-expressed genes. (**D**) Module-trait associations of module's color and disease trait. The correlation was qualified with the P-value presented at the bottom of each section. (**E**) A scatterplot of module membership and gene significance in the turquoise module

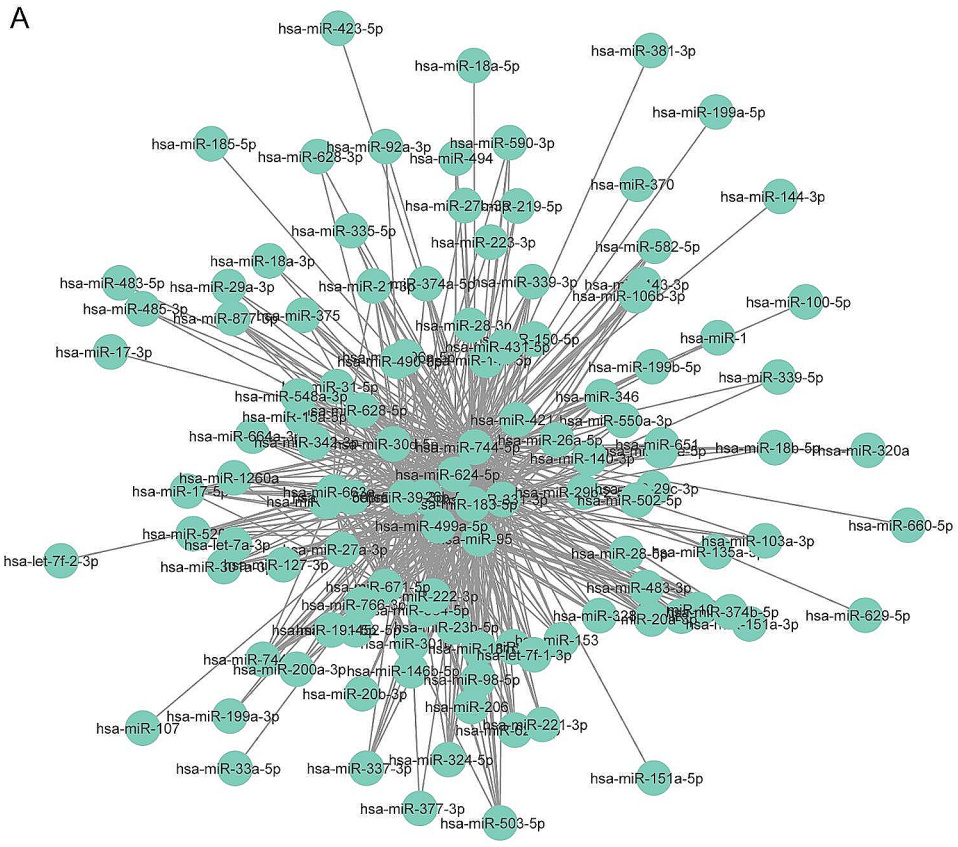

Fig. 2 The weighted co-expression networks for turquoise modules

of HUVECs. As shown in Fig. 5A-B, treatment with CM from miR-744-5p-overexpressed OS cells inhibited the viability and tube formation of HUVECs, while treatment with CM from the miR-744-5p-suppressed OS cells showed promoting effects on the cell viability and tube formation of HUVECs. These results supported the bioinformatics analysis results and confirmed that miR-744-5p inhibited the cell viability of OS cells and the tube formation of HUVECs.

Mir-744-5p directly targeted NFIX

To explore the underlying mechanism of miR-744-5p, we used TargetScan, DIANA-Tarbase, and starBase for target prediction. By taking the intersection of the prediction results, NFIX and LDL receptor-related protein 3 (LRP3) were identified as potential targets of miR-744-5p (Fig. 6A). Their expressions in miR-744-5p overexpressed OS cells were detected. The results showed that miR-744-5p overexpression significantly decreased NFIX mRNA expression while having little effect on LRP3 mRNA expression (Fig. 6B). Thus, NFIX was selected as the target of miR-744-5p in OS cells. According to the predicted binding sequences, we conducted the dual-luciferase reporter experiments and confirmed that miR-744-5p targeted NFIX in 143B cells (Fig. 6C). Additionally, the protein expression of NFIX was markedly downregulated after the transfection with miR-744-5p mimics and markedly upregulated after the transfection with miR-744-5p inhibitor, indicating that miR-744-5p could negatively regulate NFIX at the protein level (Fig. 6D). It was also found that NFIX was highly expressed in OS cells (Fig. 6E). Taken together, these data suggested that miR-744-5p targeted NFIX in OS.

NFIX attenuated the suppressive effects of mir-744-5p on the cell viability of OS cells and tube formation of HUVECs

Given the binding relationship between miR-744-5p and NFIX, whether miR-744-5p regulates the malignant phenotype of OS cells by targeting NFIX was further explored. To this end, we constructed the NFIX overexpression vector, which could promote the protein expression of NFIX in both 143B and U2OS cells (Fig. 7A). Then, the cells were co-transfected with miR-744-5p mimics and NFIX overexpression vector. As expected, the protein expression was suppressed in miR-744-5p-overexpressed cells, and co-transfection with NFIX overexpression vector restored the NFIX expression in OS cells (Fig. 7B). Subsequently, cell viability and apoptosis were detected. It was shown that the regulatory effects of miR-744-5p on cell viability and apoptosis

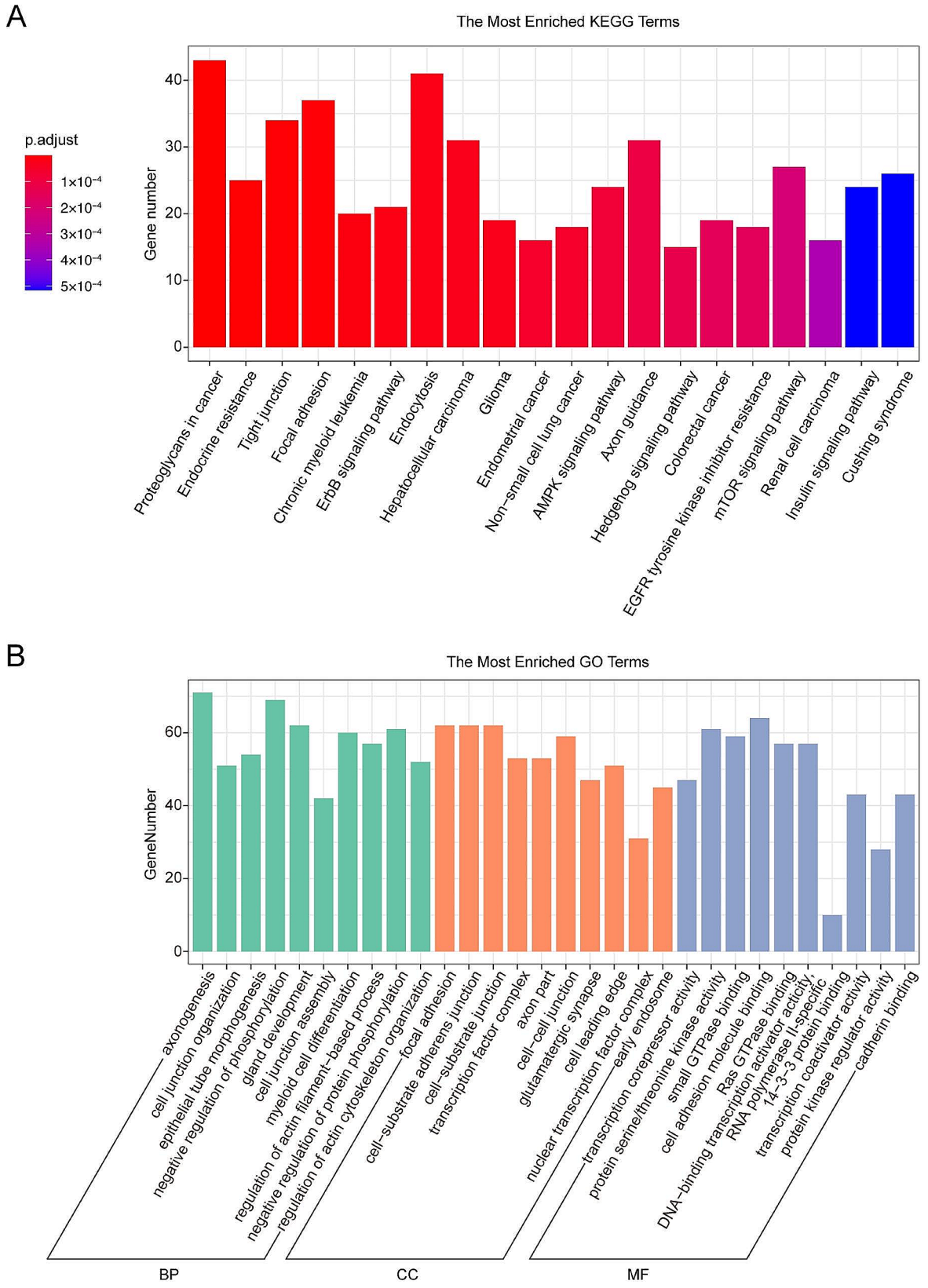

Fig. 3 Significant enriched KEGG (**A**) and GO (**B**) pathways. Each bar presents a term. BP: biological process, CC: cellular component, MF: molecular function

Table 2 KEGG analysis of miR-744-5p

ID	Description	GeneRatio	BgRatio	*P*.Value	*P*.adjust	qvalue	Count
hsa05205	Proteoglycans in cancer	43/579	205/8105	7.57×10^{-11}	2.30×10^{-8}	1.54×10^{-8}	43
hsa01522	Endocrine resistance	25/579	98/8105	1.28×10^{-8}	1.95×10^{-6}	1.31×10^{-6}	25
hsa04530	Tight junction	34/579	169/8105	2.36×10^{-8}	2.39×10^{-6}	1.61×10^{-6}	34
hsa04510	Focal adhesion	37/579	201/8105	6.65×10^{-8}	5.05×10^{-6}	3.39×10^{-6}	37
hsa05220	Chronic myeloid leukemia	20/579	76/8105	2.13×10^{-7}	1.29×10^{-5}	8.70×10^{-6}	20
hsa04012	ErbB signaling pathway	21/579	85/8105	3.40×10^{-7}	1.72×10^{-5}	1.16×10^{-5}	21
hsa04144	Endocytosis	41/579	252/8105	4.41×10^{-7}	1.92×10^{-5}	1.29×10^{-5}	41
hsa05225	Hepatocellular carcinoma	31/579	168/8105	7.46×10^{-7}	2.75×10^{-5}	1.85×10^{-5}	31
hsa05214	Glioma	19/579	75/8105	8.14×10^{-7}	2.75×10^{-5}	1.85×10^{-5}	19
hsa05213	Endometrial cancer	16/579	58/8105	1.78×10^{-6}	5.40×10^{-5}	3.62×10^{-5}	16
hsa05223	Non-small cell lung cancer	18/579	72/8105	1.95×10^{-6}	5.40×10^{-5}	3.62×10^{-5}	18
hsa04152	AMPK signaling pathway	24/579	120/8105	3.12×10^{-6}	7.91×10^{-5}	5.31×10^{-5}	24
hsa04360	Axon guidance	31/579	182/8105	4.37×10^{-6}	1.02×10^{-4}	6.86×10^{-5}	31
hsa04340	Hedgehog signaling pathway	15/579	56/8105	5.59×10^{-6}	1.21×10^{-4}	8.15×10^{-5}	15
hsa05210	Colorectal cancer	19/579	86/8105	7.36×10^{-6}	1.49×10^{-4}	1.00×10^{-4}	19
hsa01521	EGFR tyrosine kinase inhibitor resistance	18/579	79/8105	8.09×10^{-6}	1.54×10^{-4}	1.03×10^{-4}	18
hsa04150	mTOR signaling pathway	27/579	155/8105	1.19×10^{-5}	2.12×10^{-4}	1.42×10^{-4}	27
hsa05211	Renal cell carcinoma	16/579	69/8105	2.03×10^{-5}	3.43×10^{-4}	2.30×10^{-4}	16
hsa04910	Insulin signaling pathway	24/579	137/8105	3.28×10^{-5}	5.16×10^{-4}	3.47×10^{-4}	24
hsa04934	Cushing syndrome	26/579	155/8105	3.40×10^{-5}	5.16×10^{-4}	$3.47\times10_{-4}$	26
hsa05218	Melanoma	16/579	72/8105	3.57×10^{-5}	5.17×10^{-4}	3.47×10^{-4}	16
hsa05224	Breast cancer	25/579	147/8105	3.78×10^{-5}	5.23×10^{-4}	3.51×10^{-4}	25
hsa04390	Hippo signaling pathway	26/579	157/8105	4.26×10^{-5}	5.52×10^{-4}	3.71×10^{-4}	26
hsa05215	Prostate cancer	19/579	97/8105	4.48×10^{-5}	5.52×10^{-4}	3.71×10^{-4}	19
hsa04211	Longevity regulating pathway	18/579	89/8105	4.54×10^{-5}	5.52×10^{-4}	$3.71\times10-4$	18
hsa05231	Choline metabolism in cancer	19/579	98/8105	5.20×10^{-5}	6.08×10^{-4}	4.08×10^{-4}	19
hsa05221	Acute myeloid leukemia	15/579	67/8105	5.69×10^{-5}	6.41×10^{-4}	4.31×10^{-4}	15
hsa05212	Pancreatic cancer	16/579	76/8105	7.19×10^{-5}	7.81×10^{-4}	5.24×10^{-4}	16
hsa04140	Autophagy-animal	23/579	137/8105	9.43×10^{-5}	9.88×10^{-4}	6.64×10^{-4}	23
hsa05219	Bladder cancer	11/579	41/8105	9.85×10^{-5}	9.98×10^{-4}	6.70×10^{-4}	11
hsa04520	Adherens junction	15/579	71/8105	1.15×10^{-4}	1.13×10^{-3}	7.60×10^{-4}	15
hsa05163	Human cytomegalovirus infection	32/579	225/8105	1.27×10^{-4}	1.21×10^{-3}	8.10×10^{-4}	32
hsa04540	Gap junction	17/579	88/8105	1.34×10^{-4}	1.23×10^{-3}	8.28×10^{-4}	17
hsa04810	Regulation of actin cytoskeleton	31/579	218/8105	1.62×10^{-4}	1.45×10^{-3}	9.72×10^{-4}	31
hsa04370	VEGF signaling pathway	13/579	59/8105	2.09×10^{-4}	1.82×10^{-3}	1.22×10^{-3}	13
hsa04310	Wnt signaling pathway	25/579	166/8105	2.83×10^{-4}	2.39×10^{-3}	1.60×10^{-3}	25
hsa04926	Relaxin signaling pathway	21/579	129/8105	2.92×10^{-4}	2.40×10^{-3}	1.61×10^{-3}	21
hsa04068	FoxO signaling pathway	21/579	131/8105	3.63×10^{-4}	2.90×10^{-3}	1.95×10^{-3}	21
hsa04928	Parathyroid hormone synthesis, secretion and action	18/579	106/8105	4.62×10^{-4}	3.60×10^{-3}	2.42×10^{-3}	18
hsa04550	Signaling pathways regulating pluripotency of stem cells	22/579	143/8105	4.78×10^{-4}	3.63×10^{-3}	2.44×10^{-3}	22
hsa04722	Neurotrophin signaling pathway	19/579	119/8105	7.17×10^{-4}	5.27×10^{-3}	3.54×10^{-3}	19
hsa05160	Hepatitis C	23/579	157/8105	7.28×10^{-4}	5.27×10^{-3}	3.54×10^{-3}	23
hsa05226	Gastric cancer	22/579	149/8105	8.47×10^{-4}	5.99×10^{-3}	4.02×10^{-3}	22
hsa05161	Hepatitis B	23/579	162/8105	1.13×10^{-3}	7.80×10^{-3}	5.24×10^{-3}	23
hsa04917	Prolactin signaling pathway	13/579	70/8105	1.19×10^{-3}	8.03×10^{-3}	5.39×10^{-3}	13
hsa04151	PI3K-Akt signaling pathway	41/579	354/8105	1.32×10^{-3}	8.72×10^{-3}	5.86×10^{-3}	41
hsa04024	cAMP signaling pathway	28/579	216/8105	1.46×10^{-3}	9.47×10^{-3}	6.36×10^{-3}	28
hsa04933	AGE-RAGE signaling pathway in diabetic complications	16/579	100/8105	1.80×10^{-3}	1.10×10^{-2}	7.41×10^{-3}	16
hsa05166	Human T-cell leukemia virus 1 infection	28/579	219/8105	1.80×10^{-3}	1.10×10^{-2}	7.41×10^{-3}	28
hsa04072	Phospholipase D signaling pathway	21/579	148/8105	1.84×10^{-3}	1.10×10^{-2}	7.41×10^{-3}	21
hsa04071	Sphingolipid signaling pathway	18/579	119/8105	1.85×10^{-3}	1.10×10^{-2}	7.41×10^{-3}	18
hsa04015	Rap1 signaling pathway	27/579	210/8105	1.99×10^{-3}	1.15×10^{-2}	7.72×10^{-3}	27
hsa04916	Melanogenesis	16/579	101/8105	2.00×10^{-3}	1.15×10^{-2}	7.72×10^{-3}	16

Table 2 (continued)

ID	Description	GeneRatio	BgRatio	*P*.Value	*P*.adjust	qvalue	Count
hsa04912	GnRH signaling pathway	15/579	93/8105	2.28×10^{-3}	1.29×10^{-2}	8.64×10^{-3}	15
hsa04062	Chemokine signaling pathway	25/579	192/8105	2.42×10^{-3}	1.34×10^{-2}	8.99×10^{-3}	25
hsa05203	Viral carcinogenesis	26/579	204/8105	2.71×10^{-3}	1.47×10^{-2}	9.87×10^{-3}	26
hsa04137	Mitophagy - animal	12/579	68/8105	$2.85\times10-3$	1.49×10^{-2}	1.00×10^{-2}	12
hsa04664	Fc epsilon RI signaling pathway	12/579	68/8105	2.85×10^{-3}	1.49×10^{-2}	1.00×10^{-2}	12
hsa04921	Oxytocin signaling pathway	21/579	154/8105	3.01×10^{-3}	1.55×10^{-2}	1.04×10^{-2}	21
hsa04210	Apoptosis	19/579	136/8105	3.55×10^{-3}	1.80×10^{-2}	1.21×10^{-2}	19
hsa04925	Aldosterone synthesis and secretion	15/579	98/8105	3.84×10^{-3}	1.91×10^{-2}	1.28×10^{-2}	15
hsa05235	PD-L1 expression and PD-1 checkpoint pathway in cancer	14/579	89/8105	3.99×10^{-3}	1.91×10^{-2}	1.29×10^{-2}	14
hsa04931	Insulin resistance	16/579	108/8105	4.01×10^{-3}	1.91×10^{-2}	1.29×10^{-2}	16
hsa04213	Longevity regulating pathway – multiple species	11/579	62/8105	4.03×10^{-3}	1.91×10^{-2}	1.29×10^{-2}	11
hsa04014	Ras signaling pathway	28/579	232/8105	4.18×10^{-3}	1.92×10^{-2}	1.29×10^{-2}	28
hsa04915	Estrogen signaling pathway	19/579	138/8105	4.18×10^{-3}	1.92×10^{-2}	1.29×10^{-2}	19
hsa04066	HIF-1 signaling pathway	16/579	109/8105	4.40×10^{-3}	2.00×10^{-2}	1.34×10^{-2}	16
hsa00310	Lysine degradation	11/579	63/8105	4.58×10^{-3}	2.02×10^{-2}	1.35×10^{-2}	11
hsa05217	Basal cell carcinoma	11/579	63/8105	4.58×10^{-3}	2.02×10^{-2}	1.35×10^{-2}	11
hsa04662	B cell receptor signaling pathway	13/579	82/8105	5.08×10^{-3}	2.21×10^{-2}	1.48×10^{-2}	13
hsa04929	GnRH secretion	11/579	64/8105	$5.18\times10-3$	2.22×10^{-2}	1.49×10^{-2}	11
hsa04010	MAPK signaling pathway	33/579	294/8105	$6.14\times10-3$	2.59×10^{-2}	1.74×10^{-2}	33
hsa04660	T cell receptor signaling pathway	15/579	104/8105	6.75×10^{-3}	2.78×10^{-2}	1.87×10^{-2}	15
hsa04670	Leukocyte transendothelial migration	16/579	114/8105	6.83×10^{-3}	2.78×10^{-2}	1.87×10^{-2}	16
hsa05130	Pathogenic Escherichia coli infection	24/579	197/8105	6.85×10^{-3}	2.78×10^{-2}	1.87×10^{-2}	24
hsa04218	Cellular senescence	20/579	156/8105	7.49×10^{-3}	3.00×10^{-2}	2.01×10^{-2}	20
hsa04330	Notch signaling pathway	10/579	59/8105	8.32×10^{-3}	3.28×10^{-2}	2.21×10^{-2}	10
hsa04070	Phosphatidylinositol signaling system	14/579	97/8105	8.65×10^{-3}	3.33×10^{-2}	2.24×10^{-2}	14
hsa04666	Fc gamma R-mediated phagocytosis	14/579	97/8105	8.65×10^{-3}	3.33×10^{-2}	$2.24\times10-2$	14
hsa04922	Glucagon signaling pathway	15/579	107/8105	8.76×10^{-3}	3.33×10^{-2}	2.24×10^{-2}	15
hsa04920	Adipocytokine signaling pathway	11/579	69/8105	9.20×10^{-3}	3.41×10^{-2}	2.29×10^{-2}	11
hsa05031	Amphetamine addiction	11/579	69/8105	9.20×10^{-3}	3.41×10^{-2}	2.29×10^{-2}	11
hsa05230	Central carbon metabolism in cancer	11/579	70/8105	1.02×10^{-2}	3.71×10^{-2}	2.49×10^{-2}	11
hsa04935	Growth hormone synthesis, secretion and action	16/579	119/8105	1.02×10^{-2}	3.71×10^{-2}	2.49×10^{-2}	16
hsa04961	Endocrine and other factor-regulated calcium reabsorption	9/579	53/8105	1.19×10^{-2}	4.24×10^{-2}	2.85×10^{-2}	9
hsa05165	Human papillomavirus infection	35/579	331/8105	1.20×10^{-2}	4.24×10^{-2}	2.85×10^{-2}	35
hsa01524	Platinum drug resistance	11/579	73/8105	1.39×10^{-2}	4.80×10^{-2}	3.22×10^{-2}	11
hsa04115	p53 signaling pathway	11/579	73/8105	1.39×10^{-2}	4.80×10^{-2}	3.22×10^{-2}	11

were neutralized when restoring the expression of NFIX (Fig. 7C-E). Similarly, in HUVECs, transfection with miR-744-5p mimics suppressed the cell viability and tube formation of HUVECs, and this suppressive effect was weakened by the co-transfection of miR-744-5p mimics and NFIX overexpression vector (Fig. 7F-G). Above all, these results indicated that the regulatory role of miR-744-5p in OS cells and HUVECs was through mediating NFIX.

Discussion

Osteosarcoma is a malignant bone tumor that exhibits highly aggressive and rapid metastasis [32]. In the complicated pathogenesis of OS, miRNAs function as essential regulators, participating in various cellular processes such as cell proliferation, apoptosis, and angiogenesis [6, 33]. Therefore, we focused our attention on miRNAs in the current study.

To identify the key miRNA in OS progression, we used the miRNA dataset GSE65071 to conduct differential miRNA analysis and WGCNA. Ultimately, miR-744-5p was identified as the key miRNA in OS. As a multifunctional miRNA, miR-744-5p has been investigated in various cancer progressions. For example, it has been found that miR-744-5p is up-regulated in pancreatic neuroendocrine tumors (pNET) and enhances the proliferation and migration of pNET cells by inhibiting the expression of thrombospondin 2 [34]. Conversely, miR-744-5p is down-regulated in lung adenocarcinoma (LUAD). In vitro experiments have shown that miR-744-5p suppresses malignant behaviors of LUAD cells by targeting cell division cycle-associated protein 4 and MAF bZIP transcription factor G [35, 36]. Similarly, in glioma,

Table 3 GO BP analysis of miR-744-5p

ID	Description	GeneRatio	BgRatio	*P*.Value	*P*.adjust	qvalue	Count
GO:0007409	Axonogenesis	71/1214	468/18,670	1.76×10^{-11}	9.94×10^{-8}	7.74×10^{-8}	71
GO:0034330	Cell junction organization	51/1214	290/18,670	6.53×10^{-11}	1.76×10^{-7}	1.37×10^{-7}	51
GO:0060562	Epithelial tube morphogenesis	54/1214	322/18,670	1.15×10^{-10}	1.76×10^{-7}	1.37×10^{-7}	54
GO:0042326	Negative regulation of phosphorylation	69/1214	468/18,670	1.25×10^{-10}	1.76×10^{-7}	1.37×10^{-7}	69
GO:0048732	Gland development	62/1214	434/18,670	3.88×10^{-9}	3.87×10^{-6}	3.02×10^{-6}	62
GO:0034329	Cell junction assembly	42/1214	241/18,670	4.17×10^{-9}	3.87×10^{-6}	3.02×10^{-6}	42
GO:0030099	Myeloid cell differentiation	60/1214	416/18,670	4.81×10^{-9}	3.87×10^{-6}	3.02×10^{-6}	60
GO:0032970	Regulation of actin filament-based process	57/1214	388/18,670	5.96×10^{-9}	3.89×10^{-6}	3.03×10^{-6}	57
GO:0001933	Negative regulation of protein phosphorylation	61/1214	429/18,670	6.21×10^{-9}	3.89×10^{-6}	3.03×10^{-6}	61
GO:0032956	Regulation of actin cytoskeleton organization	52/1214	343/18,670	9.46×10^{-9}	5.33×10^{-6}	4.16×10^{-6}	52
GO:0051348	Negative regulation of transferase activity	45/1214	285/18,670	2.72×10^{-8}	1.32×10^{-5}	1.03×10^{-5}	45
GO:0018210	Peptidyl-threonine modification	28/1214	134/18,670	3.04×10^{-8}	1.32×10^{-5}	1.03×10^{-5}	28
GO:0018107	Peptidyl-threonine phosphorylation	27/1214	126/18,670	3.05×10^{-8}	1.32×10^{-5}	1.03×10^{-5}	27
GO:0001763	Morphogenesis of a branching structure	35/1214	196/18,670	4.29×10^{-8}	1.73×10^{-5}	1.35×10^{-5}	35
GO:0031589	Cell-substrate adhesion	51/1214	354/18,670	7.13×10^{-8}	2.68×10^{-5}	2.09×10^{-5}	51
GO:0048568	Embryonic organ development	58/1214	428/18,670	8.22×10^{-8}	2.90×10^{-5}	2.26×10^{-5}	58
GO:0034332	Adherens junction organization	28/1214	142/18,670	1.12×10^{-7}	3.71×10^{-5}	2.89×10^{-5}	28
GO:0016570	Histone modification	60/1214	454/18,670	1.21×10^{-7}	3.78×10^{-5}	2.95×10^{-5}	60
GO:0030111	Regulation of Wnt signaling pathway	51/1214	363/18,670	1.60×10^{-7}	4.46×10^{-5}	3.47×10^{-5}	51
GO:0007160	Cell-matrix adhesion	37/1214	225/18,670	1.62×10^{-7}	4.46×10^{-5}	3.47×10^{-5}	37
GO:0006469	Negative regulation of protein kinase activity	38/1214	235/18,670	1.73×10^{-7}	4.46×10^{-5}	3.47×10^{-5}	38
GO:0007265	Ras protein signal transduction	59/1214	448/18,670	1.74×10^{-7}	4.46×10^{-5}	3.47×10^{-5}	59
GO:0060070	Canonical Wnt signaling pathway	48/1214	335/18,670	2.03×10^{-7}	4.83×10^{-5}	3.77×10^{-5}	48
GO:0034333	Adherens junction assembly	21/1214	90/18,670	2.25×10^{-7}	4.83×10^{-5}	3.77×10^{-5}	21
GO:0061138	Morphogenesis of a branching epithelium	32/1214	182/18,670	2.33×10^{-7}	4.83×10^{-5}	3.77×10^{-5}	32
GO:0033673	Negative regulation of kinase activity	40/1214	257/18,670	2.36×10^{-7}	4.83×10^{-5}	3.77×10^{-5}	40
GO:0016569	Covalent chromatin modification	61/1214	474/18,670	2.44×10^{-7}	4.83×10^{-5}	3.77×10^{-5}	61
GO:0006914	Autophagy	63/1214	496/18,670	2.49×10^{-7}	4.83×10^{-5}	3.77×10^{-5}	63
GO:0061919	Process utilizing autophagic mechanism	63/1214	496/18,670	2.49×10^{-7}	4.83×10^{-5}	3.77×10^{-5}	63
GO:0051056	Regulation of small GTPase mediated signal transduction	48/1214	338/18,670	2.67×10^{-7}	5.01×10^{-5}	3.90×10^{-5}	48
GO:0007178	Transmembrane receptor protein serine/threonine kinase signaling pathway	49/1214	349/18,670	2.85×10^{-7}	5.18×10^{-5}	4.03×10^{-5}	49
GO:0009896	Positive regulation of catabolic process	56/1214	423/18,670	3.00×10^{-7}	5.29×10^{-5}	4.12×10^{-5}	56
GO:0090092	Regulation of transmembrane receptor protein serine/threonine kinase signaling pathway	38/1214	241/18,670	3.35×10^{-7}	5.72×10^{-5}	4.46×10^{-5}	38
GO:0048754	Branching morphogenesis of an epithelial tube	28/1214	150/18,670	3.69×10^{-7}	6.12×10^{-5}	4.76×10^{-5}	28
GO:0021915	Neural tube development	29/1214	160/18,670	4.39×10^{-7}	6.97×10^{-5}	5.43×10^{-5}	29
GO:0010810	Regulation of cell-substrate adhesion	35/1214	215/18,670	4.45×10^{-7}	6.97×10^{-5}	5.43×10^{-5}	35
GO:0030879	Mammary gland development	27/1214	143/18,670	4.68×10^{-7}	7.13×10^{-5}	5.56×10^{-5}	27
GO:0022604	Regulation of cell morphogenesis	61/1214	484/18,670	5.04×10^{-7}	7.48×10^{-5}	5.83×10^{-5}	61
GO:0001952	Regulation of cell-matrix adhesion	24/1214	119/18,670	5.76×10^{-7}	8.33×10^{-5}	6.49×10^{-5}	24
GO:0007050	Cell cycle arrest	37/1214	237/18,670	6.13×10^{-7}	8.63×10^{-5}	6.73×10^{-5}	37
GO:0046578	Regulation of Ras protein signal transduction	37/1214	238/18,670	6.81×10^{-7}	9.18×10^{-5}	7.15×10^{-5}	37
GO:1,901,888	Regulation of cell junction assembly	20/1214	88/18,670	6.84×10^{-7}	9.18×10^{-5}	7.15×10^{-5}	20
GO:0045666	Positive regulation of neuron differentiation	50/1214	371/18,670	7.55×10^{-7}	9.85×10^{-5}	7.68×10^{-5}	50
GO:0043087	Regulation of GTPase activity	60/1214	479/18,670	7.69×10^{-7}	9.85×10^{-5}	7.68×10^{-5}	60
GO:0007044	Cell-substrate junction assembly	21/1214	97/18,670	8.55×10^{-7}	1.07×10^{-4}	8.34×10^{-5}	21
GO:0030100	Regulation of endocytosis	41/1214	281/18,670	9.63×10^{-7}	1.18×10^{-4}	9.19×10^{-5}	41
GO:0016358	Dendrite development	36/1214	233/18,670	1.11×10^{-6}	1.34×10^{-4}	1.04×10^{-4}	36
GO:0050769	Positive regulation of neurogenesis	59/1214	474/18,670	1.17×10^{-6}	1.37×10^{-4}	1.07×10^{-4}	59
GO:0002064	Epithelial cell development	33/1214	207/18,670	1.52×10^{-6}	1.75×10^{-4}	1.36×10^{-4}	33
GO:0031331	Positive regulation of cellular catabolic process	48/1214	361/18,670	1.84×10^{-6}	2.08×10^{-4}	1.62×10^{-4}	48
GO:0051147	Regulation of muscle cell differentiation	30/1214	181/18,670	1.98×10^{-6}	2.17×10^{-4}	1.69×10^{-4}	30

Table 3 (continued)

ID	Description	GeneRatio	BgRatio	*P*.Value	*P*.adjust	qvalue	Count
GO:0043547	Positive regulation of GTPase activity	52/1214	405/18,670	2.01×10^{-6}	2.17×10^{-4}	1.69×10^{-4}	52
GO:0003007	Heart morphogenesis	38/1214	259/18,670	2.08×10^{-6}	2.21×10^{-4}	1.72×10^{-4}	38
GO:0003151	Outflow tract morphogenesis	18/1214	79/18,670	2.35×10^{-6}	2.45×10^{-4}	1.91×10^{-4}	18
GO:0061180	Mammary gland epithelium development	17/1214	72/18,670	2.65×10^{-6}	2.69×10^{-4}	2.10×10^{-4}	17
GO:0003279	Cardiac septum development	22/1214	112/18,670	2.67×10^{-6}	2.69×10^{-4}	2.10×10^{-4}	22
GO:1,903,725	Regulation of phospholipid metabolic process	19/1214	88/18,670	2.94×10^{-6}	2.90×10^{-4}	2.26×10^{-4}	19
GO:0035148	Tube formation	26/1214	148/18,670	3.13×10^{-6}	3.04×10^{-4}	2.37×10^{-4}	26
GO:0007045	Cell-substrate adherens junction assembly	18/1214	81/18,670	3.45×10^{-6}	3.24×10^{-4}	2.52×10^{-4}	18
GO:0048041	Focal adhesion assembly	18/1214	81/18,670	3.45×10^{-6}	3.24×10^{-4}	2.52×10^{-4}	18
GO:0010506	Regulation of autophagy	44/1214	327/18,670	3.59×10^{-6}	3.31×10^{-4}	2.58×10^{-4}	44
GO:0001649	Osteoblast differentiation	34/1214	225/18,670	3.64×10^{-6}	3.31×10^{-4}	2.58×10^{-4}	34
GO:0032535	Regulation of cellular component size	48/1214	370/18,670	3.69×10^{-6}	3.31×10^{-4}	2.58×10^{-4}	48
GO:0060828	Regulation of canonical Wnt signaling pathway	40/1214	286/18,670	3.81×10^{-6}	3.35×10^{-4}	2.61×10^{-4}	40
GO:0030177	Positive regulation of Wnt signaling pathway	29/1214	179/18,670	4.65×10^{-6}	4.04×10^{-4}	3.14×10^{-4}	29
GO:1,990,778	Protein localization to cell periphery	42/1214	311/18,670	5.41×10^{-6}	4.62×10^{-4}	3.60×10^{-4}	42
GO:0060840	Artery development	20/1214	100/18,670	5.65×10^{-6}	4.75×10^{-4}	3.70×10^{-4}	20
GO:0072659	Protein localization to plasma membrane	37/1214	260/18,670	5.80×10^{-6}	4.81×10^{-4}	3.75×10^{-4}	37
GO:0010975	Regulation of neuron projection development	59/1214	499/18,670	6.04×10^{-6}	4.93×10^{-4}	3.84×10^{-4}	59
GO:0031532	Actin cytoskeleton reorganization	20/1214	101/18,670	6.62×10^{-6}	5.33×10^{-4}	4.15×10^{-4}	20
GO:0032386	Regulation of intracellular transport	52/1214	423/18,670	7.15×10^{-6}	5.67×10^{-4}	4.42×10^{-4}	52
GO:0045444	Fat cell differentiation	33/1214	223/18,670	7.94×10^{-6}	6.22×10^{-4}	4.84×10^{-4}	33
GO:0033143	Regulation of intracellular steroid hormone receptor signaling pathway	17/1214	78/18,670	8.45×10^{-6}	6.52×10^{-4}	5.08×10^{-4}	17
GO:0032388	Positive regulation of intracellular transport	32/1214	215/18,670	9.60×10^{-6}	7.31×10^{-4}	5.70×10^{-4}	32
GO:0016049	Cell growth	57/1214	484/18,670	9.74×10^{-6}	7.32×10^{-4}	5.71×10^{-4}	57
GO:0090100	Positive regulation of transmembrane receptor protein serine/threonine kinase signaling pathway	20/1214	104/18,670	1.05×10^{-5}	7.78×10^{-4}	6.06×10^{-4}	20
GO:0043393	Regulation of protein binding	32/1214	217/18,670	1.17×10^{-5}	8.53×10^{-4}	6.65×10^{-4}	32
GO:0001841	Neural tube formation	20/1214	105/18,670	1.22×10^{-5}	8.80×10^{-4}	6.86×10^{-4}	20
GO:0019216	Regulation of lipid metabolic process	50/1214	410/18,670	1.33×10^{-5}	9.27×10^{-4}	7.22×10^{-4}	50
GO:0048736	Appendage development	28/1214	179/18,670	1.33×10^{-5}	9.27×10^{-4}	7.22×10^{-4}	28
GO:0060173	Limb development	28/1214	179/18,670	1.33×10^{-5}	9.27×10^{-4}	7.22×10^{-4}	28
GO:1,903,829	Positive regulation of cellular protein localization	42/1214	324/18,670	1.50×10^{-5}	1.02×10^{-3}	7.94×10^{-4}	42
GO:0090287	Regulation of cellular response to growth factor stimulus	39/1214	292/18,670	1.50×10^{-5}	1.02×10^{-3}	7.94×10^{-4}	39
GO:0003205	Cardiac chamber development	27/1214	171/18,670	1.59×10^{-5}	1.06×10^{-3}	8.22×10^{-4}	27
GO:0060444	Branching involved in mammary gland duct morphogenesis	9/1214	25/18,670	1.59×10^{-5}	1.06×10^{-3}	8.22×10^{-4}	9
GO:0048146	Positive regulation of fibroblast proliferation	13/1214	51/18,670	1.62×10^{-5}	1.06×10^{-3}	8.27×10^{-4}	13
GO:0001843	Neural tube closure	18/1214	90/18,670	1.64×10^{-5}	1.06×10^{-3}	8.27×10^{-4}	18
GO:0030326	Embryonic limb morphogenesis	22/1214	125/18,670	1.70×10^{-5}	1.08×10^{-3}	8.39×10^{-4}	22
GO:0035113	Embryonic appendage morphogenesis	22/1214	125/18,670	1.70×10^{-5}	1.08×10^{-3}	8.39×10^{-4}	22
GO:0030168	Platelet activation	25/1214	153/18,670	1.78×10^{-5}	1.10×10^{-3}	8.58×10^{-4}	25
GO:0042176	Regulation of protein catabolic process	47/1214	381/18,670	1.78×10^{-5}	1.10×10^{-3}	8.58×10^{-4}	47
GO:0060606	Tube closure	18/1214	91/18,670	1.92×10^{-5}	1.16×10^{-3}	9.04×10^{-4}	18
GO:0001667	Ameboidal-type cell migration	54/1214	461/18,670	1.93×10^{-5}	1.16×10^{-3}	9.04×10^{-4}	54
GO:0048706	Embryonic skeletal system development	22/1214	126/18,670	1.94×10^{-5}	1.16×10^{-3}	9.04×10^{-4}	22
GO:1,903,391	Regulation of adherens junction organization	15/1214	67/18,670	2.02×10^{-5}	1.20×10^{-3}	9.31×10^{-4}	15
GO:0031346	Positive regulation of cell projection organization	47/1214	383/18,670	2.04×10^{-5}	1.20×10^{-3}	9.31×10^{-4}	47
GO:0007411	Axon guidance	37/1214	276/18,670	2.27×10^{-5}	1.31×10^{-3}	1.02×10^{-3}	37
GO:0051893	Regulation of focal adhesion assembly	14/1214	60/18,670	2.30×10^{-5}	1.31×10^{-3}	1.02×10^{-3}	14
GO:0090109	Regulation of cell-substrate junction assembly	14/1214	60/18,670	2.30×10^{-5}	1.31×10^{-3}	1.02×10^{-3}	14
GO:0042692	Muscle cell differentiation	47/1214	385/18,670	2.33×10^{-5}	1.31×10^{-3}	1.02×10^{-3}	47

Table 4 GO CC analysis of miR-744-5p

ID	Description	GeneRatio	BgRatio	*P*.Value	*P*.adjust	qvalue	Count
GO:0005925	Focal adhesion	62/1253	405/19,717	9.71×10^{-11}	4.33×10^{-8}	3.61×10^{-8}	62
GO:0005924	Cell-substrate adherens junction	62/1253	408/19,717	1.32×10^{-10}	4.33×10^{-8}	3.61×10^{-8}	62
GO:0030055	Cell-substrate junction	62/1253	412/19,717	1.99×10^{-10}	4.33×10^{-8}	3.62×10^{-8}	62
GO:0005667	Transcription factor complex	53/1253	365/19,717	1.45×10^{-8}	2.36×10^{-6}	1.97×10^{-6}	53
GO:0033267	Axon part	53/1253	382/19,717	6.77×10^{-8}	8.85×10^{-6}	7.39×10^{-6}	53
GO:0005911	Cell-cell junction	59/1253	459/19,717	1.89×10^{-7}	2.07×10^{-5}	1.73×10^{-5}	59
GO:0098978	Glutamatergic synapse	47/1253	349/19,717	8.84×10^{-7}	8.26×10^{-5}	6.90×10^{-5}	47
GO:0031252	Cell leading edge	51/1253	403/19,717	2.02×10^{-6}	1.65×10^{-4}	1.38×10^{-4}	51
GO:0044798	Nuclear transcription factor complex	31/1253	201/19,717	4.00×10^{-6}	2.91×10^{-4}	2.43×10^{-4}	31
GO:0005769	Early endosome	45/1253	350/19,717	5.25×10^{-6}	3.43×10^{-4}	2.87×10^{-4}	45
GO:0042641	Actomyosin	17/1253	79/19,717	7.51×10^{-6}	4.46×10^{-4}	3.73×10^{-4}	17
GO:0030426	Growth cone	27/1253	171/19,717	1.06×10^{-5}	5.77×10^{-4}	4.82×10^{-4}	27
GO:0000118	Histone deacetylase complex	14/1253	58/19,717	1.18×10^{-5}	5.92×10^{-4}	4.95×10^{-4}	14
GO:0017053	Transcriptional repressor complex	17/1253	84/19,717	1.77×10^{-5}	7.89×10^{-4}	6.59×10^{-4}	17
GO:0030427	Site of polarized growth	27/1253	176/19,717	1.81×10^{-5}	7.89×10^{-4}	6.59×10^{-4}	27
GO:1,990,907	Beta-catenin-TCF complex	6/1253	11/19,717	2.28×10^{-5}	9.31×10^{-4}	7.78×10^{-4}	6
GO:0031256	Leading edge membrane	26/1253	170/19,717	2.71×10^{-5}	1.03×10^{-3}	8.61×10^{-4}	26
GO:0150034	Distal axon	37/1253	285/19,717	2.84×10^{-5}	1.03×10^{-3}	8.61×10^{-4}	37
GO:0030863	Cortical cytoskeleton	20/1253	116/19,717	3.99×10^{-5}	1.37×10^{-3}	1.15×10^{-3}	20
GO:0005938	Cell cortex	38/1253	308/19,717	6.84×10^{-5}	2.24×10^{-3}	1.87×10^{-3}	38
GO:0044304	Main axon	14/1253	68/19,717	7.88×10^{-5}	2.44×10^{-3}	2.04×10^{-3}	14
GO:0043025	Neuronal cell body	54/1253	497/19,717	8.20×10^{-5}	2.44×10^{-3}	2.04×10^{-3}	54
GO:0090575	RNA polymerase II transcription factor complex	24/1253	163/19,717	1.01×10^{-4}	2.86×10^{-3}	2.39×10^{-3}	24
GO:0044448	Cell cortex part	26/1253	184/19,717	1.06×10^{-4}	2.89×10^{-3}	2.41×10^{-3}	26
GO:0010008	Endosome membrane	52/1253	479/19,717	1.13×10^{-4}	2.95×10^{-3}	2.46×10^{-3}	52
GO:0030864	Cortical actin cytoskeleton	16/1253	90/19,717	1.59×10^{-4}	3.99×10^{-3}	3.33×10^{-3}	16
GO:0014069	Postsynaptic density	38/1253	324/19,717	1.98×10^{-4}	4.46×10^{-3}	3.73×10^{-3}	38
GO:0016581	NuRD complex	6/1253	15/19,717	1.98×10^{-4}	4.46×10^{-3}	3.73×10^{-3}	6
GO:0090545	CHD-type complex	6/1253	15/19,717	1.98×10^{-4}	4.46×10^{-3}	3.73×10^{-3}	6
GO:0098984	Neuron to neuron synapse	40/1253	350/19,717	2.35×10^{-4}	5.12×10^{-3}	4.28×10^{-3}	40
GO:0032279	Asymmetric synapse	38/1253	328/19,717	2.53×10^{-4}	5.34×10^{-3}	4.46×10^{-3}	38
GO:0032587	Ruffle membrane	16/1253	94/19,717	2.67×10^{-4}	5.45×10^{-3}	4.56×10^{-3}	16
GO:0000790	Nuclear chromatin	42/1253	377/19,717	2.88×10^{-4}	5.71×10^{-3}	4.77×10^{-3}	42
GO:0000792	Heterochromatin	14/1253	78/19,717	3.61×10^{-4}	6.95×10^{-3}	5.81×10^{-3}	14
GO:0098562	Cytoplasmic side of membrane	24/1253	178/19,717	3.91×10^{-4}	7.31×10^{-3}	6.11×10^{-3}	24
GO:0099572	Postsynaptic specialization	39/1253	348/19,717	4.15×10^{-4}	7.53×10^{-3}	6.29×10^{-3}	39
GO:0030139	Endocytic vesicle	35/1253	303/19,717	4.60×10^{-4}	8.14×10^{-3}	6.80×10^{-3}	35
GO:0044291	Cell-cell contact zone	13/1253	71/19,717	4.75×10^{-4}	8.18×10^{-3}	6.83×10^{-3}	13
GO:1,902,911	Protein kinase complex	17/1253	109/19,717	5.05×10^{-4}	8.47×10^{-3}	7.08×10^{-3}	17
GO:0098793	Presynapse	50/1253	491/19,717	6.75×10^{-4}	1.10×10^{-2}	9.22×10^{-3}	50
GO:0097060	Synaptic membrane	45/1253	432/19,717	7.68×10^{-4}	1.23×10^{-2}	1.02×10^{-2}	45
GO:0070603	SWI/SNF superfamily-type complex	13/1253	76/19,717	9.30×10^{-4}	1.39×10^{-2}	1.16×10^{-2}	13
GO:0001725	Stress fiber	12/1253	67/19,717	9.51×10^{-4}	1.39×10^{-2}	1.16×10^{-2}	12
GO:0097517	Contractile actin filament bundle	12/1253	67/19,717	9.51×10^{-4}	1.39×10^{-2}	1.16×10^{-2}	12
GO:0005774	Vacuolar membrane	43/1253	412/19,717	9.56×10^{-4}	1.39×10^{-2}	1.16×10^{-2}	43
GO:0005765	Lysosomal membrane	38/1253	354/19,717	1.10×10^{-3}	1.57×10^{-2}	1.31×10^{-2}	38
GO:0005913	Cell-cell adherens junction	17/1253	117/19,717	1.15×10^{-3}	1.58×10^{-2}	1.32×10^{-2}	17
GO:0098852	Lytic vacuole membrane	38/1253	355/19,717	1.16×10^{-3}	1.58×10^{-2}	1.32×10^{-2}	38
GO:0030673	Axolemma	5/1253	14/19,717	1.27×10^{-3}	1.69×10^{-2}	1.41×10^{-2}	5
GO:0031253	Cell projection membrane	37/1253	345/19,717	1.29×10^{-3}	1.69×10^{-2}	1.41×10^{-2}	37
GO:0001726	Ruffle	22/1253	172/19,717	1.36×10^{-3}	1.74×10^{-2}	1.46×10^{-2}	22
GO:0005770	Late endosome	29/1253	256/19,717	1.83×10^{-3}	2.26×10^{-2}	1.88×10^{-2}	29
GO:0009898	Cytoplasmic side of plasma membrane	20/1253	154/19,717	1.83×10^{-3}	2.26×10^{-2}	1.88×10^{-2}	20

Table 4 (continued)

ID	Description	GeneRatio	BgRatio	*P*.Value	*P*.adjust	qvalue	Count
GO:0030666	Endocytic vesicle membrane	21/1253	167/19,717	2.13×10^{-3}	2.58×10^{-2}	2.16×10^{-2}	21
GO:0098839	Postsynaptic density membrane	12/1253	74/19,717	2.31×10^{-3}	2.75×10^{-2}	2.30×10^{-2}	12
GO:0000932	P-body	13/1253	84/19,717	2.38×10^{-3}	2.78×10^{-2}	2.33×10^{-2}	13
GO:0097197	Tetraspanin-enriched microdomain	4/1253	10/19,717	2.50×10^{-3}	2.87×10^{-2}	2.40×10^{-2}	4
GO:0032432	Actin filament bundle	12/1253	75/19,717	2.60×10^{-3}	2.93×10^{-2}	2.45×10^{-2}	12
GO:0030135	Coated vesicle	31/1253	289/19,717	3.05×10^{-3}	3.38×10^{-2}	2.82×10^{-2}	31
GO:0097440	Apical dendrite	5/1253	17/19,717	3.34×10^{-3}	3.64×10^{-2}	3.04×10^{-2}	5
GO:1,902,554	Serine/threonine protein kinase complex	13/1253	88/19,717	3.62×10^{-3}	3.88×10^{-2}	3.24×10^{-2}	13
GO:0030136	Clathrin-coated vesicle	22/1253	188/19,717	4.16×10^{-3}	4.38×10^{-2}	3.66×10^{-2}	22
GO:0016327	Apicolateral plasma membrane	5/1253	18/19,717	4.39×10^{-3}	4.55×10^{-2}	3.80×10^{-2}	5

Table 5 GO MF analysis of miR-744-5p

ID	Description	GeneRatio	BgRatio	*P*.Value	*P*.adjust	qvalue	Count
GO:0003714	Transcription corepressor activity	47/1227	238/17,697	5.11×10^{-11}	4.97×10^{-8}	4.47×10^{-8}	47
GO:0004674	Protein serine/threonine kinase activity	61/1227	439/17,697	1.45×10^{-7}	7.06×10^{-5}	6.35×10^{-5}	61
GO:0031267	Small GTPase binding	59/1227	443/17,697	9.78×10^{-7}	3.13×10^{-4}	2.81×10^{-4}	59
GO:0050839	Cell adhesion molecule binding	64/1227	499/17,697	1.29×10^{-6}	3.13×10^{-4}	2.81×10^{-4}	64
GO:0017016	Ras GTPase binding	57/1227	429/17,697	1.61×10^{-6}	3.13×10^{-4}	2.81×10^{-4}	57
GO:0001228	DNA-binding transcription activator activity, RNA polymerase II-specific	57/1227	439/17,697	3.33×10^{-6}	5.39×10^{-4}	4.85×10^{-4}	57
GO:0071889	14-3-3 protein binding	10/1227	29/17,697	1.47×10^{-5}	2.03×10^{-3}	1.83×10^{-3}	10
GO:0003713	Transcription coactivator activity	43/1227	319/17,697	2.11×10^{-5}	2.56×10^{-3}	2.30×10^{-3}	43
GO:0019887	Protein kinase regulator activity	28/1227	180/17,697	4.65×10^{-5}	4.98×10^{-3}	4.47×10^{-3}	28
GO:0045296	Cadherin binding	43/1227	331/17,697	5.12×10^{-5}	4.98×10^{-3}	4.47×10^{-3}	43
GO:0019207	Kinase regulator activity	30/1227	207/17,697	9.72×10^{-5}	8.58×10^{-3}	7.72×10^{-3}	30
GO:0001227	DNA-binding transcription repressor activity, RNA polymerase II-specific	32/1227	242/17,697	3.25×10^{-4}	2.63×10^{-2}	2.37×10^{-2}	32
GO:0017137	Rab GTPase binding	25/1227	175/17,697	4.46×10^{-4}	3.34×10^{-2}	3.00×10^{-2}	25
GO:0005522	Profilin binding	5/1227	11/17,697	5.16×10^{-4}	3.58×10^{-2}	3.22×10^{-2}	5
GO:0001221	Transcription cofactor binding	10/1227	43/17,697	5.76×10^{-4}	3.73×10^{-2}	3.35×10^{-2}	10
GO:0017124	SH3 domain binding	20/1227	130/17,697	6.22×10^{-4}	3.73×10^{-2}	3.35×10^{-2}	20
GO:0005096	GTPase activator activity	34/1227	273/17,697	6.52×10^{-4}	3.73×10^{-2}	3.35×10^{-2}	34
GO:0005178	Integrin binding	20/1227	132/17,697	7.59×10^{-4}	4.10×10^{-2}	3.68×10^{-2}	20
GO:0019902	Phosphatase binding	25/1227	185/17,697	1.02×10^{-3}	4.68×10^{-2}	4.21×10^{-2}	25
GO:0001085	RNA polymerase II transcription factor binding	22/1227	155/17,697	1.04×10^{-3}	4.68×10^{-2}	4.21×10^{-2}	22
GO:0030295	Protein kinase activator activity	14/1227	80/17,697	1.11×10^{-3}	4.68×10^{-2}	4.21×10^{-2}	14
GO:0046332	SMAD binding	14/1227	80/17,697	1.11×10^{-3}	4.68×10^{-2}	4.21×10^{-2}	14
GO:0004860	Protein kinase inhibitor activity	12/1227	63/17,697	1.15×10^{-3}	4.68×10^{-2}	4.21×10^{-2}	12
GO:0005088	Ras guanyl-nucleotide exchange factor activity	20/1227	137/17,697	1.22×10^{-3}	4.68×10^{-2}	4.21×10^{-2}	20
GO:0030291	Protein serine/threonine kinase inhibitor activity	8/1227	32/17,697	1.22×10^{-3}	4.68×10^{-2}	4.21×10^{-2}	8
GO:0051015	Actin filament binding	26/1227	198/17,697	1.25×10^{-3}	4.68×10^{-2}	4.21×10^{-2}	26

miR-744-5p is expressed at low levels and acts as a tumor suppressor by inhibiting the polarization of macrophages M2 [37]. Additionally, recent studies have reported that miR-744-5p can reduce the resistance of gastric cancer cells to PD-L1 by inhibiting immune escape [38], and decrease the resistance of non-small cell lung cancer cells to cisplatin by promoting ferroptosis [39]. Here, we observed a down-regulated expression of miR-744-5p in OS cells. In addition, overexpression of miR-744-5p inhibited the cell proliferation of OS cells, which is consistent with the previous study [24]. Therefore, miR-744-5p is a prime candidate for tumor suppressive factors in OS.

GO analysis showed that miR-744-5p was enriched in angiogenesis, which is the process of developing new blood vessels and is essential for the progression of many types of tumors [40]. One of the characteristics of OS is the dense blood vessels [41]. Prior research has shown that miRNA miR-429 and miR-206 directly mitigate the angiogenesis of HUVECs to exert the anti-tumor effect in OS [42]. Another study reported that miR-877-3p attenuates the angiogenesis of HUVECs to exhibit a

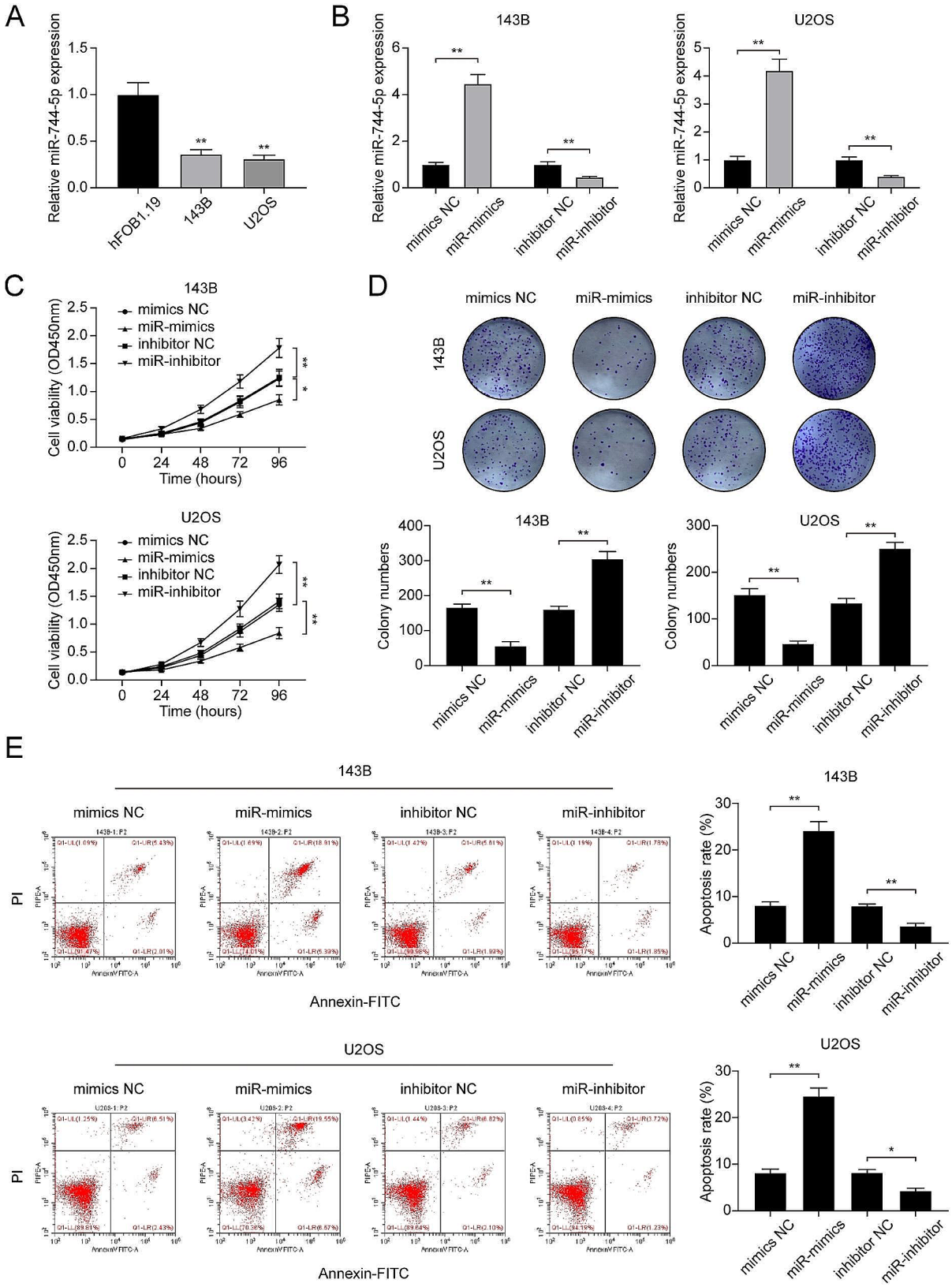

Fig. 4 miR-744-5p inhibited the viability of osteosarcoma cells. (**A**) Expression levels of miR-744-5p in OS cells and normal endothelial cells. (**B**) The transfection efficiency was verified by qRT-PCR. (**C**) CCK-8 assay was applied to determine the viability of OS cells. (**D**) In vitro cell clonogenicity was examined by colony formation assay. (**E**) Cell apoptosis rate was evaluated by flow cytometry. *$P < 0.05$; ** $P < 0.01$

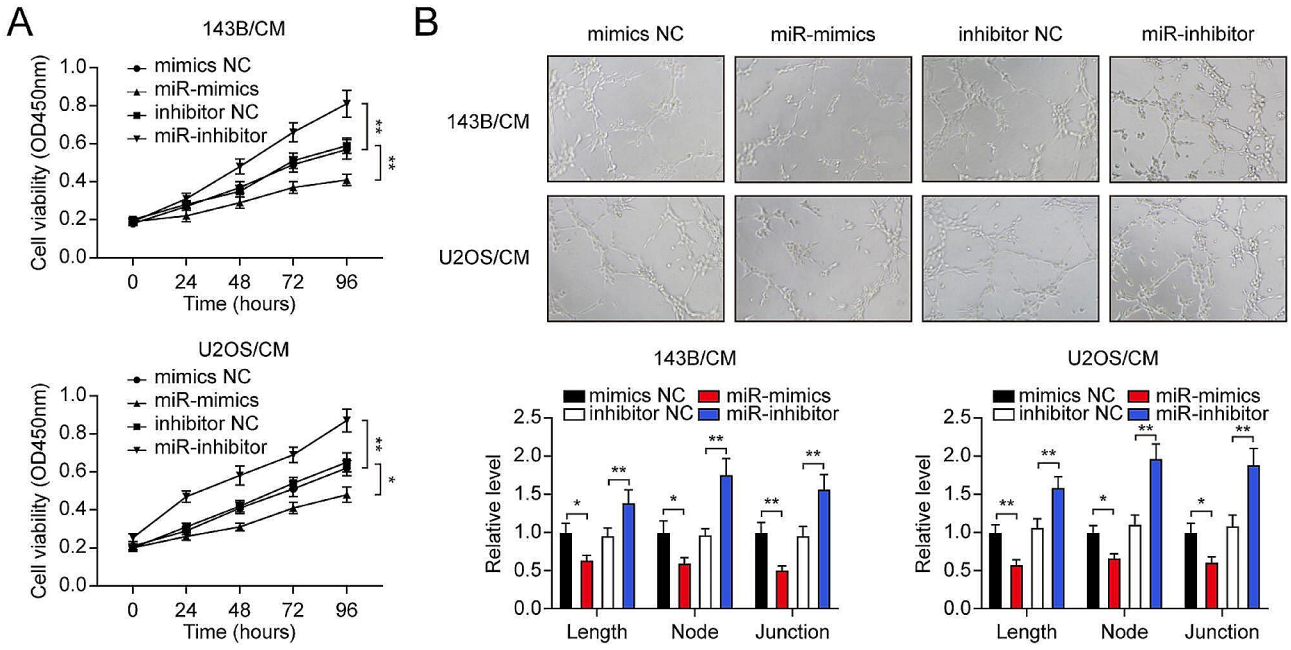

Fig. 5 miR-744-5p contained the viability and tube formation of HUVECs. (**A**) Cell viability of HUVECs was detected by CCK-8 assay. (**B**) Tube formation assay was performed in HUVECs. *$P < 0.05$; ** $P < 0.01$

tumor-suppressive role in OS [43]. Although miR-744-5p has been reported to inhibit cell proliferation, migration, and invasion in various cancers, there have been no studies on its role in regulating the angiogenesis of HUVECs. In the current study, we confirmed the regulation of miR-744-5p on the cell viability and tube formation of HUVECs by treating the HUVECs with CM from the OS cells. We found that treatment with CM from miR-744-5p-overexpressed OS cells inhibited the viability and tube formation of HUVECs, whereas treatment with CM from miR-744-5p-suppressed OS cells showed opposite effects. To the best of our knowledge, this is the first study to provide evidence of the regulation of miR-744-5p on the angiogenesis of HUVECs.

During tumor-induced angiogenesis, the tumor-derived extracellular vesicles (EVs) play important roles [44, 45]. EVs are heterogeneous particles that are secreted by cells into the extracellular environment. Based on the size, biogenesis, and function, the EVs can be classified into exosomes, macrovesicles, and apoptotic bodies [46]. Recently, researchers isolated EVs from cells' CM and found that EVs actively engage in intercellular communication through the transfer of intracellular cargos such as proteins and nucleic acids [47–49]. Specifically, miRNAs released by EVs can be uptake by other cells, thus influencing the various physiopathological conditions [44]. For example, EVs-derived miR-141-3p, miR-21-5p, and miR-210-3p are reported to facilitate endothelial cell angiogenesis [50–52]. Zhang et al. reported that miR-199a-5p is down-regulated in osteosarcoma plasma samples compared with normal plasma samples. Through exosomes, miR-199a-5p can be transported from OS cells to HUVECs, thereby inhibiting HUVEC proliferation, migration, and neovascularization [53]. These results suggest that the mechanism that miR-744-5p regulates the angiogenesis of HUVECs may be through the EVs-dependent manner. OS cells secreted miR-744-5p into the cell culture medium via EVs. Then, EVs containing miR-744-5p could enter HUVECs to regulate the proliferation and angiogenesis of HUVECs. Delivery of EVs-derived miR-744-5p, such as mesenchymal stem cell-derived EVs-miR-744-5p [37], may be a preventive strategy against angiogenesis in OS. However, caution should be exercised when targeting a tumor suppressor miRNA as a therapeutic target unless the miRNA can be delivered to a specific site [54]. Thus, further investigation on the EVs-miR-744-5p is needed to elucidate its complicated roles in OS initiation and progression.

Besides, in most cases, the regulatory mechanism of miRNAs is to bind to the 3'untranslated region of the target genes to inhibit their expression [55]. Previous studies have shown that miR-744-5p targets ADP ribosylation factor 1, SRY-box transcription factor 12, replication factor C subunit 2, and others to suppress the progression of several types of cancer [56–58]. In the current study, we used TargetScan, DIANA-Tarbase, and starBase algorithms to predict miR-744-5p targets and identified NFIX as the target gene of miR-744-5p in OS. Studies have identified the essential role of NFIX in hematopoiesis [59], muscle development [60], and brain

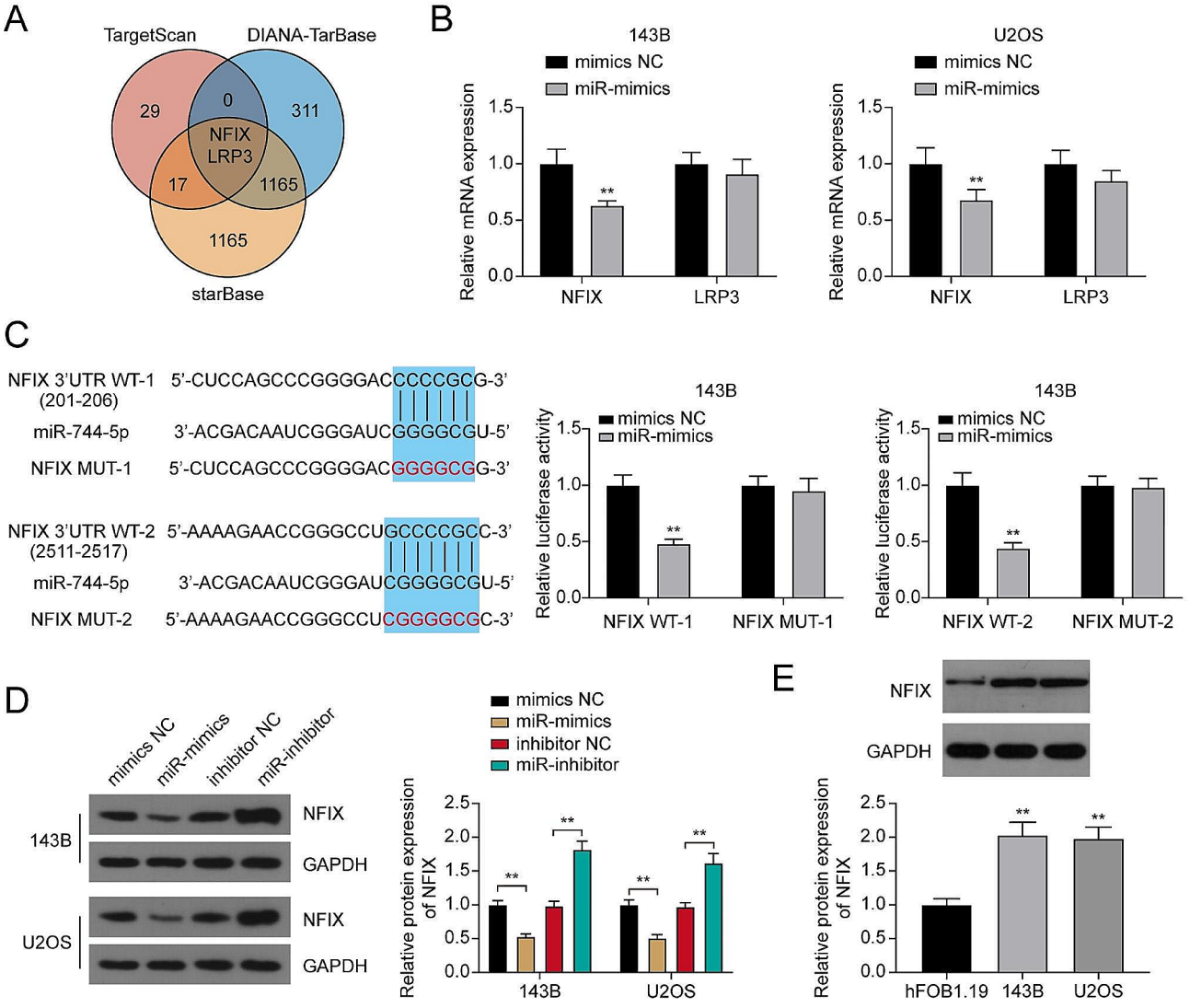

Fig. 6 miR-744-5p directly targets NFIX. (**A**) TargetScan, DIANA-Tarbase, and starBase algorithms were applied to identify potential downstream targets of miR-744-5p. (**B**) NFIX mRNA expression in OS cells transfected with miR-744-5p mimics. (**C**) Wild type and mutant binding sequences of miR-744-5p on NFIX. The direct binding was verified by dual-luciferase reporter assay. (**D**) NFIX protein expression in OS cells transfected with miR-744-5p mimics and miR-744-5p inhibitor. (**E**) NFIX protein expression in OS cells. ** $P < 0.01$

development [61]. However, little is known about its role in tumor development. Previous research on lung cancer has found that NFIX inhibition reduces cell proliferation, migration, and invasion in vitro [28]. Another study reported that NFIX is mediated by miR-3196 to exacerbate the progression of pancreatic cancer [62]. In this study, we revealed that NFIX is overexpressed in OS cells. Moreover, NFIX overexpression neutralized the suppressive effects of miR-744-5p on the viability of OS cells and angiogenesis in HUVECs. These results are consistent with the previous observation that miR-744-5p negatively regulates NFIX to inhibit cell viability in ovarian cancer [18]. Our study revealed the association of miR-744-5p with NFIX in the OS progression and provided evidence for the importance of the miR-744-5p/NFIX axis in inhibiting OS cell growth and HUVECs angiogenesis. On considering the use of RNA interference technology in human diseases in recent years [63–65], targeting the miR-744-5p/NFIX axis may have potential application in the OS treatment.

This study had some limitations. We focused on the downstream regulatory mechanism of miR-744-5p in the current study. The mechanisms that suppress the miR-744-5p expression in OS have not been investigated. For example, long non-coding RNA MNX1-AS1 and LINC01116 bind to miR-744-5p and inhibit its expression in ovarian cancer and pituitary adenoma [57, 66]. Promoter methylation and transcriptional inhibition by transcription factors are also reported to be directly associated with suppressed miRNA expression [67, 68].

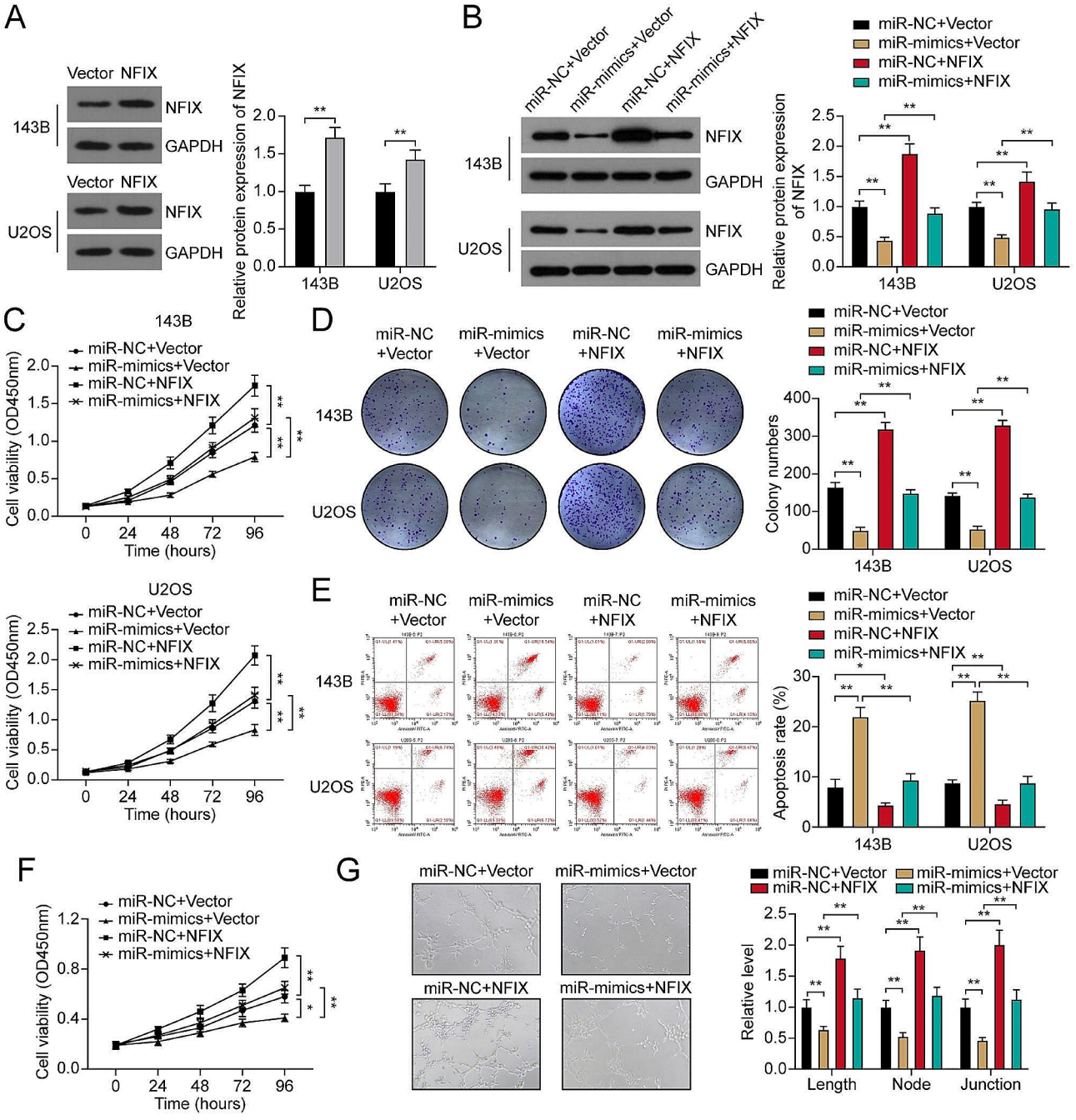

Fig. 7 NFIX neutralized the effects of miR-744-5p on osteosarcoma cells. (**A**) Protein expression of NFIX in OS cells transfected with NFIX overexpression vector. (**B**) Protein expression of NFIX in different groups of OS cells. (**C**) OS cell viability was assessed by CCK-8 assay. (**D**) Cell proliferation was visualized by colony formation assay. (**E**) Flow cytometry assay was performed to determine cell apoptosis rate. (**F**) The viability of HUVECs was assessed by CCK-8 assay. (**G**) The effects of miR-744-5p and NFIX on the tube formation of HUVECs were detected by tube formation assay. **P* < 0.05; ** *P* < 0.01

Additional investigations are warranted to unveil the mechanisms that regulate the expression of miR-744-5p in OS. Besides, we confirmed the roles of the miR-744-5p/NFIX axis on OS cells viability and HUVECs angiogenesis based on the in vitro assays. However, these results require further validation by clinical OS samples and in vivo studies such as subcutaneous injection or orthotopic models. Furthermore, the precise mechanism of miR-744-5p/NFIX in regulating the OS cells viability and HUVECs angiogenesis is still unclear, which needs further confirmation in the follow-up studies.

Conclusion

Taken together, we revealed the miR-744-5p/NFIX axis in osteosarcoma. MiR-744-5p overexpression could restrain osteosarcoma cell viability and HUVECs angiogenesis by targeting inhibition of NFIX. Our results highlight the significance of miR-744-5p as a potential target for osteosarcoma treatment.

Acknowledgements
Not applicable.

Author contributions
All authors contributed to the study conception and design. Material preparation, data collection and analysis were performed by Lin Xie, Wei Li and Yu Li. The first draft of the manuscript was written by Lin Xie and Yu Li. All authors commented on previous versions of the manuscript. All authors read and approved the final manuscript.

Funding
The authors declare that no funds, grants, or other support were received during the preparation of this manuscript.

Data availability
No datasets were generated or analysed during the current study.

Declarations

Ethical approval
None.

Consent to participate
None.

Competing interests
The authors declare no competing interests.

Received: 13 April 2024 / Accepted: 23 July 2024
Published online: 17 August 2024

References

1. Cortini M, Avnet S, Baldini N. Mesenchymal stroma: role in osteosarcoma progression. Cancer Lett. 2017;405:90–9.
2. Isakoff MS, Bielack SS, Meltzer P, et al. Osteosarcoma: current treatment and a collaborative pathway to Success. J Clin Oncol. 2015;33:3029–35.
3. van Maldegem AM, Bhosale A, Gelderblom HJ, et al. Comprehensive analysis of published phase I/II clinical trials between 1990–2010 in osteosarcoma and Ewing sarcoma confirms limited outcomes and need for translational investment. Clin Sarcoma Res. 2012;2:5.
4. Meltzer PS, Helman LJ. New Horizons in the Treatment of Osteosarcoma. N Engl J Med. 2021;385:2066–76.
5. Wang J, Liu S, Shi J, et al. The role of miRNA in the diagnosis, prognosis, and treatment of Osteosarcoma. Cancer Biother Radiopharm. 2019;34:605–13.
6. Zhang J, Yan YG, Wang C, et al. MicroRNAs in osteosarcoma. Clin Chim Acta. 2015;444:9–17.
7. Hammond SM. An overview of microRNAs. Adv Drug Deliv Rev. 2015;87:3–14.
8. He L, Hannon GJ. MicroRNAs: small RNAs with a big role in gene regulation. Nat Rev Genet. 2004;5:522–31.
9. Giordano L, Porta GD, Peretti GM, et al. Therapeutic potential of microRNA in tendon injuries. Br Med Bull. 2020;133:79–94.
10. Oliviero A, Della Porta G, Peretti GM, et al. MicroRNA in osteoarthritis: physiopathology, diagnosis and therapeutic challenge. Br Med Bull. 2019;130:137–47.
11. Wang F, Zhao QH, Liu JZ, et al. MiRNA-188-5p alleviates the progression of osteosarcoma via target degrading CCNT2. Eur Rev Med Pharmacol Sci. 2020;24:29–35.
12. Gao G, Tian Z, Zhu HY, et al. miRNA-133b targets FGFR1 and presents multiple tumor suppressor activities in osteosarcoma. Cancer Cell Int. 2018;18:210.
13. Lv Y, Wu L, Jian H, et al. Identification and characterization of aging/senescence-induced genes in osteosarcoma and predicting clinical prognosis. Front Immunol. 2022;13:997765.
14. Jiang Y, Wang J, Sun M, et al. Multi-omics analysis identifies osteosarcoma subtypes with distinct prognosis indicating stratified treatment. Nat Commun. 2022;13:7207.
15. Liu D, Wang H, Zhou Z, et al. Integrated bioinformatic analysis and experiment confirmation of the antagonistic effect and molecular mechanism of ginsenoside Rh2 in metastatic osteosarcoma. J Pharm Biomed Anal. 2021;201:114088.
16. Langfelder P, Horvath S. WGCNA: an R package for weighted correlation network analysis. BMC Bioinformatics. 2008;9:559.
17. Tian H, Guan D, Li J. Identifying osteosarcoma metastasis associated genes by weighted gene co-expression network analysis (WGCNA). Med (Baltim). 2018;97:e10781.
18. Kleemann M, Schneider H, Unger K, et al. MiR-744-5p inducing cell death by directly targeting HNRNPC and NFIX in ovarian cancer cells. Sci Rep. 2018;8:9020.
19. Fan X, Sun Y, Guo X, et al. Long non-coding RNA LINC01116 regulated miR-744-5p/SCN1B axis to exacerbate lung squamous cell carcinoma. Cancer Biomark. 2020;28:473–82.
20. Guo B, Xiao C, Liu Y, et al. Mir-744-5p inhibits multiple Myeloma Proliferation, Epithelial Mesenchymal Transformation and Glycolysis by Targeting SOX12/Wnt/beta-Catenin signaling. Onco Targets Ther. 2021;14:1161–72.
21. Yuan Q, Fan Y, Liu Z, et al. Mir-744-5p mediates lncRNA HOTTIP to regulate the proliferation and apoptosis of papillary thyroid carcinoma cells. Exp Cell Res. 2020;392:112024.
22. Huang W, Chen Q, Dai J, et al. Mir-744-5p suppresses tumor proliferation and metastasis by targeting transforming growth factor-beta 1 (TGF-beta1) in hepatocellular carcinoma (HCC). J Gastrointest Oncol. 2021;12:1811–22.
23. Ma B, Ren G, Xu J, et al. LncRNA MNX1-AS1 contributes to laryngeal squamous cell Carcinoma Growth and Migration by regulating mir-744-5p/bcl9/beta-Catenin Axis. Cell Transpl. 2021;30:9636897211005682.
24. Liang H, Li L, Zhu S, et al. MicroRNA-744-5p suppresses tumorigenesis and metastasis of osteosarcoma through the p38 mitogen-activated protein kinases pathway by targeting transforming growth factor-beta 1. Bioengineered. 2022;13:12309–25.
25. Ribeiro V, Martins SG, Lopes AS et al. NFIXing Cancer: the role of NFIX in oxidative stress response and cell fate. Int J Mol Sci 2023, 24.
26. Chen KS, Lim JWC, Richards LJ, et al. The convergent roles of the nuclear factor I transcription factors in development and cancer. Cancer Lett. 2017;410:124–38.
27. Liu Z, Ge R, Zhou J, et al. Nuclear factor IX promotes glioblastoma development through transcriptional activation of Ezrin. Oncogenesis. 2020;9:39.
28. Rahman NIA, Abdul Murad NA, Mollah MM, et al. NFIX as a Master Regulator for Lung Cancer Progression. Front Pharmacol. 2017;8:540.
29. Allen-Rhoades W, Kurenbekova L, Satterfield L, et al. Cross-species identification of a plasma microRNA signature for detection, therapeutic monitoring, and prognosis in osteosarcoma. Cancer Med. 2015;4:977–88.
30. Yu G, Wang LG, Han Y, et al. clusterProfiler: an R package for comparing biological themes among gene clusters. OMICS. 2012;16:284–7.
31. Chen Z, Xu W, Zhang D, et al. circCAMSAP1 promotes osteosarcoma progression and metastasis by sponging mir-145-5p and regulating FLI1 expression. Mol Ther Nucleic Acids. 2021;23:1120–35.
32. Ottaviani G, Jaffe N. The epidemiology of osteosarcoma. Cancer Treat Res. 2009;152:3–13.
33. Sun L, Liu M, Luan S, et al. MicroRNA-744 promotes carcinogenesis in osteosarcoma through targeting LATS2. Oncol Lett. 2019;18:2523–9.
34. Jiao H, Zeng L, Zhang J, et al. THBS2, a microRNA-744-5p target, modulates MMP9 expression through CUX1 in pancreatic neuroendocrine tumors. Oncol Lett. 2020;19:1683–92.
35. Sui Y, Lin G, Zheng Y, et al. LncRNA MAFG-AS1 boosts the proliferation of lung adenocarcinoma cells via regulating miR-744-5p/MAFG axis. Eur J Pharmacol. 2019;859:172465.
36. Ren P, Chang L, Hong X, et al. Long non-coding RNA LINC01116 is activated by EGR1 and facilitates lung adenocarcinoma oncogenicity via targeting miR-744-5p/CDCA4 axis. Cancer Cell Int. 2021;21:292.
37. Liu L, Cheng M, Zhang T, et al. Mesenchymal stem cell-derived extracellular vesicles prevent glioma by blocking M2 polarization of macrophages

through a miR-744-5p/TGFB1-dependent mechanism. Cell Biol Toxicol. 2022;38:649–65.
38. Shan H, Zhang X, Zhang X, et al. CircSCUBE3 reduces the anti-gastric Cancer activity of Anti-PD-L1. Mol Biotechnol. 2024;66:123–37.
39. Han B, Liu Y, Zhang Q, et al. Propofol decreases cisplatin resistance of non-small cell lung cancer by inducing GPX4-mediated ferroptosis through the miR-744-5p/miR-615-3p axis. J Proteom. 2023;274:104777.
40. Folkman J. The role of angiogenesis in tumor growth. Semin Cancer Biol. 1992;3:65–71.
41. Quan GM, Choong PF. Anti-angiogenic therapy for osteosarcoma. Cancer Metastasis Rev. 2006;25:707–13.
42. Zhu Y, Liu Z, Cao L, et al. FRS2 regulated by miR-429 and miR-206 promotes angiogenesis in osteosarcoma. Gene. 2024;898:148118.
43. Chen M, Li Z, Cao L, et al. Mir-877-3p inhibits tumor growth and angiogenesis of osteosarcoma through fibroblast growth factor 2 signaling. Bioengineered. 2022;13:8174–86.
44. Zhang L, Yu D. Exosomes in cancer development, metastasis, and immunity. *Biochim Biophys*. Acta Rev Cancer. 2019;1871:455–68.
45. Liu J, Ren L, Li S, et al. The biology, function, and applications of exosomes in cancer. Acta Pharm Sin B. 2021;11:2783–97.
46. Kang T, Atukorala I, Mathivanan SJN. New frontiers: extracellular vesicles. Biogenesis of extracellular vesicles; 2021. pp. 19–43.
47. Yang K, Zhang J, Bao C. Exosomal circEIF3K from cancer-associated fibroblast promotes colorectal cancer (CRC) progression via miR-214/PD-L1 axis. BMC Cancer. 2021;21:933.
48. Marton S, Miquel E, Acosta-Rodriguez J, et al. SOD1(G93A) astrocyte-derived Extracellular vesicles Induce Motor Neuron death by a miRNA-155-5p-Mediated mechanism. ASN Neuro. 2023;15:17590914231197527.
49. Choi JY, Seok HJ, Lee DH, et al. Tumor-derived mir-6794-5p enhances cancer growth by promoting M2 macrophage polarization. Cell Commun Signal. 2024;22:190.
50. Liao Z, Chen Y, Duan C, et al. Cardiac telocytes inhibit cardiac microvascular endothelial cell apoptosis through exosomal miRNA-21-5p-targeted cdip1 silencing to improve angiogenesis following myocardial infarction. Theranostics. 2021;11:268–91.
51. Wang H, Wang L, Zhou X et al. OSCC Exosomes Regulate miR-210-3p Targeting EFNA3 to Promote Oral Cancer Angiogenesis through the PI3K/AKT Pathway. *Biomed Res Int* 2020, 2020:2125656.
52. Masoumi-Dehghi S, Babashah S, Sadeghizadeh M. microRNA-141-3p-containing small extracellular vesicles derived from epithelial ovarian cancer cells promote endothelial cell angiogenesis through activating the JAK/STAT3 and NF-kappaB signaling pathways. J Cell Commun Signal. 2020;14:233–44.
53. Plouet J, Moro F, Bertagnolli S, et al. Extracellular cleavage of the vascular endothelial growth factor 189-amino acid form by urokinase is required for its mitogenic effect. J Biol Chem. 1997;272:13390–6.
54. O'Neill CP, Dwyer RM. Nanoparticle-based delivery of tumor suppressor microRNA for Cancer Therapy. Cells 2020, 9.
55. Valencia-Sanchez MA, Liu J, Hannon GJ, et al. Control of translation and mRNA degradation by miRNAs and siRNAs. Genes Dev. 2006;20:515–24.
56. Zhao LG, Wang J, Li J, et al. Mir-744-5p inhibits cellular proliferation and invasion via targeting ARF1 in epithelial ovarian cancer. Kaohsiung J Med Sci. 2020;36:799–807.
57. Shen Y, Lv M, Fang Y, et al. LncRNA MNX1-AS1 promotes ovarian cancer process via targeting the miR-744-5p/SOX12 axis. J Ovarian Res. 2021;14:161.
58. Fan F, Yao D, Yan P, et al. MicroRNA-744-5p inhibits glioblastoma malignancy by suppressing replication factor C subunit 2. Oncol Lett. 2021;22:608.
59. Walker M, Li Y, Morales-Hernandez A, et al. An NFIX-mediated regulatory network governs the balance of hematopoietic stem and progenitor cells during hematopoiesis. Blood Adv. 2023;7:4677–89.
60. Taglietti V, Angelini G, Mura G et al. RhoA and ERK signalling regulate the expression of the transcription factor nfix in myogenic cells. Development 2018, 145.
61. Fraser J, Essebier A, Gronostajski RM, et al. Cell-type-specific expression of NFIX in the developing and adult cerebellum. Brain Struct Funct. 2017;222:2251–70.
62. Ye L, Feng W, Weng H, et al. MAFG-AS1 aggravates the progression of pancreatic cancer by sponging miR-3196 to boost NFIX. Cancer Cell Int. 2020;20:591.
63. Gargano G, Oliviero A, Oliva F, et al. Small interfering RNAs in tendon homeostasis. Br Med Bull. 2021;138:58–67.
64. Gargano G, Oliva F, Oliviero A, et al. Small interfering RNAs in the management of human rheumatoid arthritis. Br Med Bull. 2022;142:34–43.
65. Gargano G, Asparago G, Spiezia F, et al. Small interfering RNAs in the management of human osteoporosis. Br Med Bull. 2023;148:58–69.
66. Huang T, Cai M, Chen C, et al. LINC01116 boosts the progression of pituitary adenoma via regulating miR-744-5p/HOXB8 pathway. Mol Cell Endocrinol. 2021;536:111350.
67. Yan Z, Ao X, Liang X, et al. Transcriptional inhibition of mir-486-3p by BCL6 upregulates snail and induces epithelial-mesenchymal transition during radiation-induced pulmonary fibrosis. Respir Res. 2022;23:104.
68. Ye S, Xiong F, He X, et al. DNA hypermethylation-induced miR-182 silence targets BCL2 and HOXA9 to facilitate the self-renewal of leukemia stem cell, accelerate acute myeloid leukemia progression, and determine the sensitivity of BCL2 inhibitor venetoclax. Theranostics. 2023;13:77–94.

Publisher's Note

Springer Nature remains neutral with regard to jurisdictional claims in published maps and institutional affiliations.